Historic, Archive Document

Do not assume content reflects current scientific knowledge, policies, or practices.

Reserve
A99.9
F7632U

Numerical Simulation of Jet Roof Geometry for Snow Cornice Control

K.L. Dawson and T.E. Lang

Research Paper RM-206
Rocky Mountain Forest
and Range Experiment Station
Forest Service
U.S. Department of Agriculture

Abstract

A numerical solution algorithm is used to study the air flow over a mountain ridge with and without a jet roof located near the ridge crest. For the simple ridge geometry studied the roof should be parallel to the lee slope, the leading edge of the roof should be at or near the ridge crest, and the height of the leading edge above ground should be about the same dimension as the roof length from leading edge to trailing edge.

Research Paper RM-206

March 1979

Numerical Simulation of Jet Roof Geometry for Snow Cornice Control[1]

K.L. Dawson, Graduate Student[2]
Montana State University

T.E. Lang, Professor
Montana State University

[1]*This research was conducted under Cooperative Agreement 16-627-CA between the Rocky Mountain Forest and Range Experiment Station, with central headquarters maintained at Fort Collins, in cooperation with Colorado State University, and Montana State University, Bozeman.*

[2]*Current affiliation: Research Engineer, Boeing Aircraft Company, Seattle, Wash.*

Contents

Numerical Simulation of Jet Roof Geometry for Snow Cornice Control[1]

K.L. Dawson and T.E. Lang

Management Implications

In many areas, snow cornices and the snow "cushion" that often forms downslope from them present serious safety problems. Snow avalanches triggered by falling cornice blocks or by failure in the snow cushion are common on such slopes. Strategic placement of a simple wind deflector, called a jet roof, at the ridge crest will often alleviate the problem by deflecting the wind down the lee slope and preventing or reducing the formation of the cornice and changing the snow deposition pattern on the slope. This paper gives information regarding the location and shape of such structures based on a computer program modeling of wind flow patterns over the ridge.

Introduction

In this report, we consider the flow of air and snow over a simplified mountain ridge and the resulting accumulation and dispersion of snow on the downwind slope. The snow cornice (fig. 1) and its closely associated, downslope snow cushion often are important factors in avalanche release. Although jet roofs have been used to change the air flow and snow deposition patterns to try to prevent cornice development, no analytical studies have been made of the optimum size and shape of these roofs.

The objective of the present research is to use a numerical solution algorithm to investigate the flow of air over a mountain ridge with a jet roof situated near the ridge crest (fig. 2). The effect the jet roof has on cornice development and the scoured region produced by the roof are evaluated. A comparison is made between the accumulation effects with and without the jet roof. Also considered is the optimization of the length and angular inclination of the jet roof with respect to the local geometry of the upper part of the lee slope. The uphill or leading edge of the jet roof is positioned relative to the crestline of the ridge, so that well defined flow is established above and beneath the roof surface, and roof angle and length are optimized. Then, using the optimum length-angle configuration of the roof, position of the roof on the slope is varied to assess its position effect on the flow.

The flow model that is used in the computer simulation is that of a laminar, rotational (or viscous) fluid in two dimensions. In using a laminar flow model, it is assumed that steadiness of the flow is a more dominant characteristic in establishing scour and stagnation regions than possible turbulence of the flow.

This paper is intended to illustrate an analytical method for studying cornice control without getting into the specifics of particular ridge geometries.

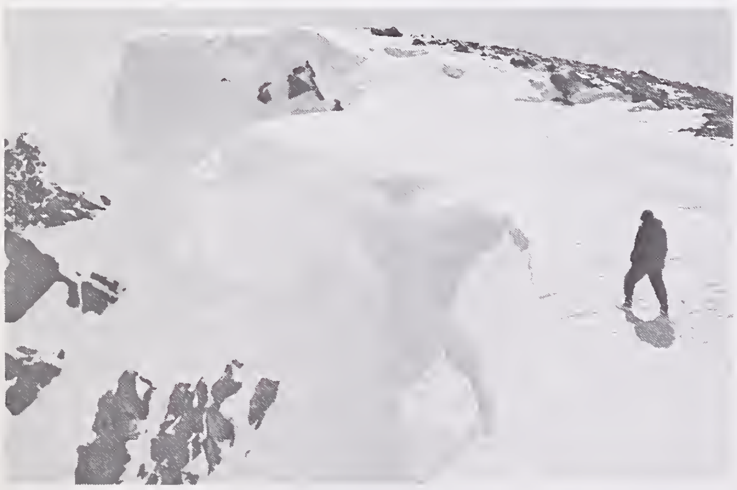

Figure 1.—A snow cornice formed where the wind decreases in the lee of a flat-topped ridge. Winds blow from right to left.

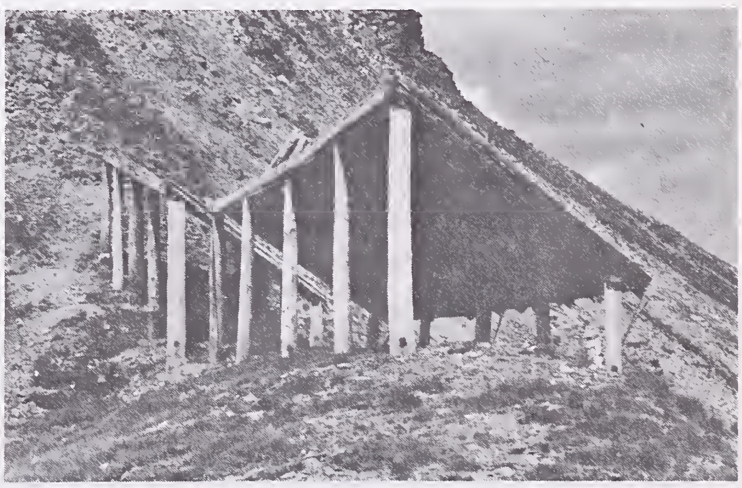

Figure 2.—A jet roof located above the lee slope. Winds trapped between the roof and the terrain are accelerated enough to prevent cornice formation.

Methodology

Since the jet roof problem involves the flow of a snow-air mixture at relatively low velocities, fluid flow is assumed incompressible. Therefore, the time-dependent fluid flow of the jet roof problem can be mathematically modeled using numerical techniques. A numerical solution algorithm (SOLA) for laminar, transient incompressible fluid flows, developed by Hirt et al. (1975), treats the problem of viscous and inviscid fluid flows in problems involving confined regions (SOLA), as well as free surfaces (SOLA-SURF). Program SOLA-SURF and its extension to admit free surfaces and curved rigid boundaries is used exclusiveley in the investigation of the jet-roof problem.

Equations of Motion

The mathematical techniques used in the SOLA-SURF code are identical to those utilized in the well-known Marker-And-Cell (MAC) method (Harlow et al. 1966). The technique uses a finite difference formulation in a two-dimensional Eulerian vector space in which the motion of the fluid particles is studied as they pass through a fixed coordinated system. The primary dependent variables are pressure and velocity.

The equations of motion which must be solved are the Navier-Stokes equations in two-dimensional Cartesian coordinates. These are written as,

$$\frac{\partial u}{\partial t}+\frac{\partial u^2}{\partial x}+\frac{\partial uv}{\partial y}=-\frac{\partial p}{\partial y}+g_x+\nu\nabla^2 u$$

$$\frac{\partial v}{\partial t}+\frac{\partial uv}{\partial x}+\frac{\partial v^2}{\partial y}=-\frac{\partial p}{\partial y}+g_y+\nu\nabla^2 v \qquad [1]$$

Also, the continuity-of-mass equation must be satisfied and is given by,

$$\underline{\nabla}\cdot\underline{V}=\frac{\partial u}{\partial x}+\frac{\partial v}{\partial y}=0 \qquad [2]$$

The x- and y-components of velocity and body acceleration are u and v, and g_x and g_y, respectively. The ratio of pressure to constant density is p, and the constant ν is the coefficient of kinematic viscosity. The Laplacian operator is ∇^2, so that, for example

$$\nabla^2 u=\frac{\partial^2 u}{\partial x^2}+\frac{\partial^2 u}{\partial y^2} \qquad [3]$$

The Navier-Stokes equations (eq. [1]) form a relationship between the flux of momentum in a fluid flow and the accelerations and viscous forces applied to the fluid. The continuity-of-mass equation, for an incompressible fluid, simply states that there is to be no net inflow of fluid with respect to time.

Finite Difference Model

The finite difference mesh used to obtain a numerical solution to equations [1] and [2] above consists of a grid of rectangular cells each of width δx and height δy. The arrangement of the finite difference variables u, v, and p in a typical cell located in the ith column and jth row is shown in figure 3.

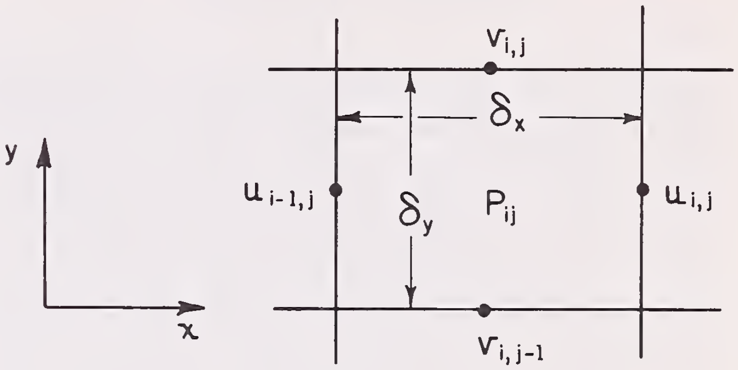

Figure 3.—Finite difference variables u, δ, and p in a typical cell in the ith column and the jth row.

The fluid flow region is divided into a gridwork of cells numbering IBAR in the x-direction and JBAR in the y-direction. The fluid flow region is surrounded by a layer of fictitious cells called phantom or boundary cells. This layer of fictitious cells is necessary when writing the finite difference equations and imposing boundary conditions. The arrangement of the overall finite difference grid is shown in figure 4 with the boundary cells located around the periphery of the fluid flow region.

Eq. [1] and [2] are given in their finite difference form by Hirt, et al. (1975). A coefficient, α, is used in the finite difference form of the Navier-Stokes equations to control the amount of upstream or "donor cell" differencing, referring to the amount of convective fluxing of momentum from an upstream cell (i-1,j) to its adjacent downstream cell (i,j). The choice of the parameter α is important when considering the numerical stability of the finite difference equations. The problem of numerical stability in the SOLA-SURF code is discussed in greater detail later.

Since finite differencing of nonlinear partial differential equations is an approximating technique, the velocities predicted by the finite difference form of the Navier-Stokes equations usually will not satisfy the continuity-of-mass equation (eq. [2]). The divergence of a cell, $\underline{\nabla}\cdot\underline{V}$, can be forced to be equal to zero by adjusting iteratively the pressure of a cell so there will be no net inflow or outflow of mass. For example, a negative divergence of a particular cell

corresponds to a net flow of mass into the cell, and the cell pressure may be increased to eliminate this inflow. Because an iterative procedure is used to force the divergence of each cell in the computational mesh to zero, a user-specified parameter, ε, must be selected as an acceptable level of accuracy for the cell divergence. The parameter, ε, describes how close to zero we wish to force the cell divergence of equation [2].

Boundary Conditions

Four types of boundary conditions are made available for use in the SOLA-SURF code. These are

1. Rigid free-slip boundary.
2. Rigid no-slip boundary.
3. Continuative boundary.
4. Periodic boundary.

Only the first and third are needed when modeling the jet roof problem. Consider the free-slip boundary condition for the bottom boundary (fig. 4). For the free-slip boundary condition, the normal velocity at the bottom boundary is zero, and the tangential velocity will have no gradient normal to the surface. Therefore,

$$u_{i,1} = u_{i,2}$$

$$v_{i,1} = 0$$

for all i.

Consider the continuative boundary condition at the right boundary (fig. 4). It is desirable to specify a continuative outflow condition at this boundary so that there will be a minimum effect on the flow preceding the boundary. We then write

$$u_{IM1,j} = u_{IM2,j}$$

$$v_{IMAX,j} = v_{IM1,j}$$

for all j, IM1 = IMAX-1, and IM2 = IMAX-2.

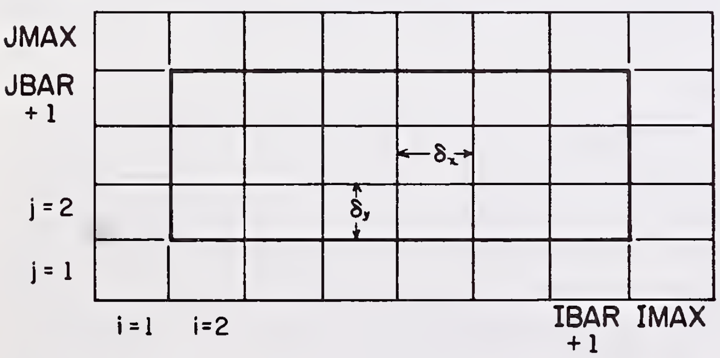

Figure 4.—Finite difference grid arrangement and nomenclature.

Two other boundary conditions are introduced in the SOLA-SURF code, and are applied when updating the configuration of free surfaces or adjusting velocities at rigid boundaries. At a free surface, the pressure must be zero. At a no-slip, rigid boundary, the velocity parallel to the boundary is zero. A detailed discussion of these boundary conditions and the updating of free surface configurations is given in Hirt et al. 1975.

Numerical Stability

When performing numerical computations, the problem of numerical instability becomes extremely important. Instability arises when variables calculated from finite difference equations develop large, uncontrolled oscillations about a solution as the computations proceed. Generally, these oscillations lead to an exponentially growing instability. A finite difference equation, especially one that is written from a nonlinear differential equation, may yield an oscillating and growing solution that does not resemble the expected solution.

The solution algorithm used to consider the jet roof problem solves the nonlinear Navier-Stokes equations numerically. To maintain numerical stability of the finite difference form of these equations, care must be exercised in selecting the cell width, δx, and height, δy, by time increment, δt, and the donor cell differencing parameter, α, discussed previously.

The mesh increments, δx and δy, must be small enough to have acceptable spatial resolution to handle variations in all of the dependent variables (velocity, pressure, and free-surface height). Experience is a valuable asset when selecting values of δx and δy. Limits placed on the allowable computing time or available memory place restrictions on how small the mesh increments may be. However, if the mesh increments are too large, the accuracy of the results may be questionable.

The selection of the time increment, δt, is governed by two restrictions, both in the form of inequalities. The first is that fluid cannot flow through more than one cell in one time step. This is because the finite difference equations are written so that mass is exchanged between adjacent cells only in a single time step. Therefore, the time increment, δt, must satisfy the inequality,

$$\delta t < \min \left\{ \frac{\delta x}{|u|}, \frac{\delta y}{|v|} \right\} \quad [4]$$

Usually, δt is chosen to be ⅓ to ½ of the minimum cell transition time predicted by equation [4]. The second restriction is used when the kinematic viscosity ν is nonzero. In this case, momentum cannot pass

through more than one cell in one time step. It can be shown that this restriction implies that

$$\nu \delta t < \frac{1}{2} \frac{\delta x^2 \delta y^2}{\delta x^2 + \delta y^2} \qquad [5]$$

Finally, the first restriction is used to predict a value for the upstream differencing parameter, α. This being the case, α is given by the inequality

$$1 \geqslant \alpha > \max \left\{ \left| \frac{u\delta t}{\delta x} \right| \quad \left| \frac{v\delta t}{\delta y} \right| \right\} \qquad [6]$$

Usually, α is taken to be 1.2 to 1.5 times the right-hand side of equation [6]. When α is taken to be zero, the finite difference equations for the Navier-Stokes equations are space centered and are numerically unstable, unless some nonzero value of kinematic viscosity, ν, is specified (Hirt 1968). When α is taken equal to 1.0, the finite difference equations reduce to the full donor cell form. These equations are stable, provided the restriction of equation [4] is satisfied.

The three inequalities given by equations [4], [5], and [6] have been added to the SOLA-SURF code, so that time, t, will be incremented automatically with the proper value of the time increment, δt, being computed each cycle. The upstream differencing parameter, α, is also adjusted accordingly. These modifications to the time advance section of the code ensure numerical stability, as far as the two restrictions placed on the flow of mass and momentum through cells are concerned. However, other problems regarding numerical instability arise when modeling the jet roof problem. These are discussed later.

Additionally, the SOLA-SURF code, which contains the options for free and curved rigid surfaces, imposes two other conditions in order to assure stability of the finite difference equations. First, the free or curved rigid surfaces, which are initially defined by the user, must remain single-valued functions $y=y(x,t)$ for all time. The second restriction is that the cell aspect ratio, $\delta y/\delta x$, may not exceed the slope of either the top or bottom surface.

The Jet Roof Problem and Its Mathematical Model

Mathematical Model

A finite difference grid is constructed in the local flow region using a two-dimensional rectangular Cartesian coordinate system. A number of simplifying refinements are made on how the jet roof flow problem is modeled to make the most effective and economic use of computer storage space and problem running time. These modifications are described below.

For simplicity, the mountain ridge geometry considered has a 45° inclination to either side of the crest (fig. 5). This simplification, although not normally physically realistic, allows the use of equal mesh increments, δx and δy which tends to speed up the convergence of the calculations, particularly during flow initiation. This simple geometry is used also to gain insight into the way flow patterns of the continuum change with respect to time when flowing past a projecting obstacle such as a mountain ridge. To represent the mountain, velocities in the cells occupied by the mountain are set equal to zero for all time in a section of the code set aside for special boundary conditions. Additionally, since the magnitude and direction of the corresponding velocity vectors for each cell are computed, these are also set equal to zero on each iteration for those cells occupied by the mountain. The same procedure is used to "zero-out" those cells occupied by the jet roof. The inclusion of both the upwind and downwind slopes in the finite difference model gives an overall picture of the development of flow patterns across the ridge. A velocity-vector plot showing the development of the flow for the "full-ridge" model is shown in figure 6.

From the results of figure 6, note that directly above the apex (or ridge crest) the velocity vectors are horizontal, as would be expected in laminar steady flow. This implies that the upwind geometry of the mountain has no influence on the flow pattern from the ridge crest downstream past the jet roof. Thus, the geometry of the mountain can be of any slope from horizontal to any angle (45° in fig. 6), and the results of the flow study past the jet roof will be the same. From the standpoint of flow continuity, upwind geometry of the mountain will affect the magnitude of the flow velocity at the ridge crest; however, in the present study this velocity is set at 20 m/s as a typical value.

The independence of solution of flow past the jet roof from upwind mountain geometry is further exemplified in a second refinement of simply shifting the ridge crest to the left-hand boundary, so that only the downwind portion of the ridge remains in the grid.

The primary advantage of this modification is a savings in computer storage space and program run time. The modifications to the code for this type of slope configuration are straightforward. The development of the flow for this "half-ridge" flow model and a jet roof length of 3.5 m is given in figure 7.

An additional refinement made to the finite difference model allows a closer look at the flow in the immediate vicinity of the jet roof. This modified form of the flow model yields a magnified view of the flow under and downslope from the jet roof, and is

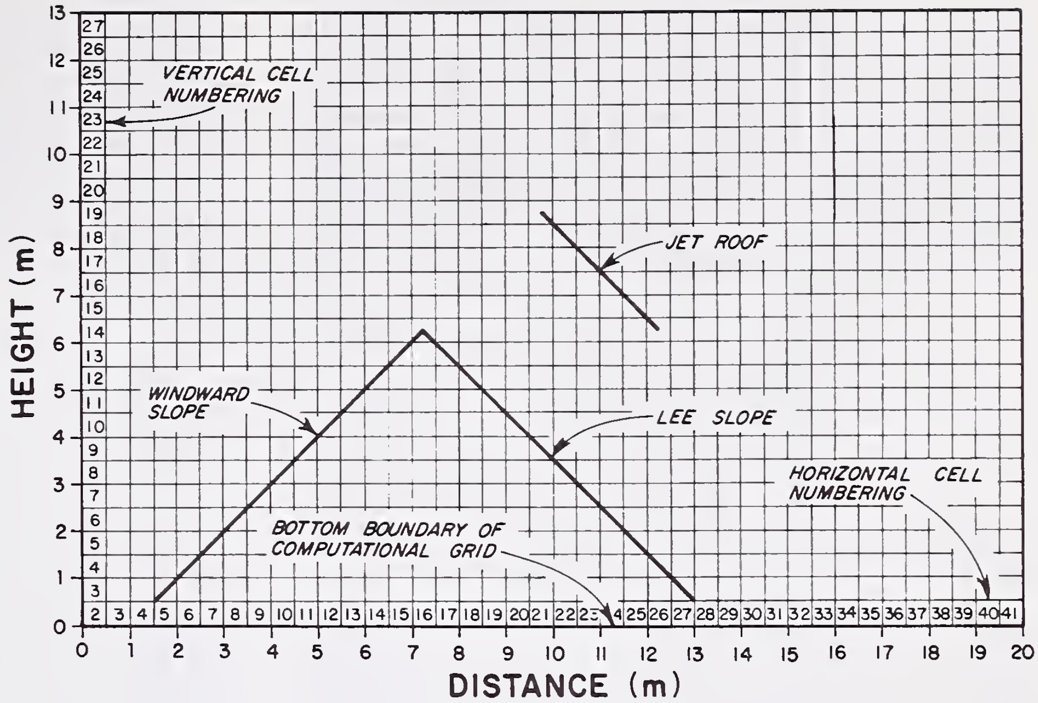

Figure 5.—Jet roof initial model (full ridge).

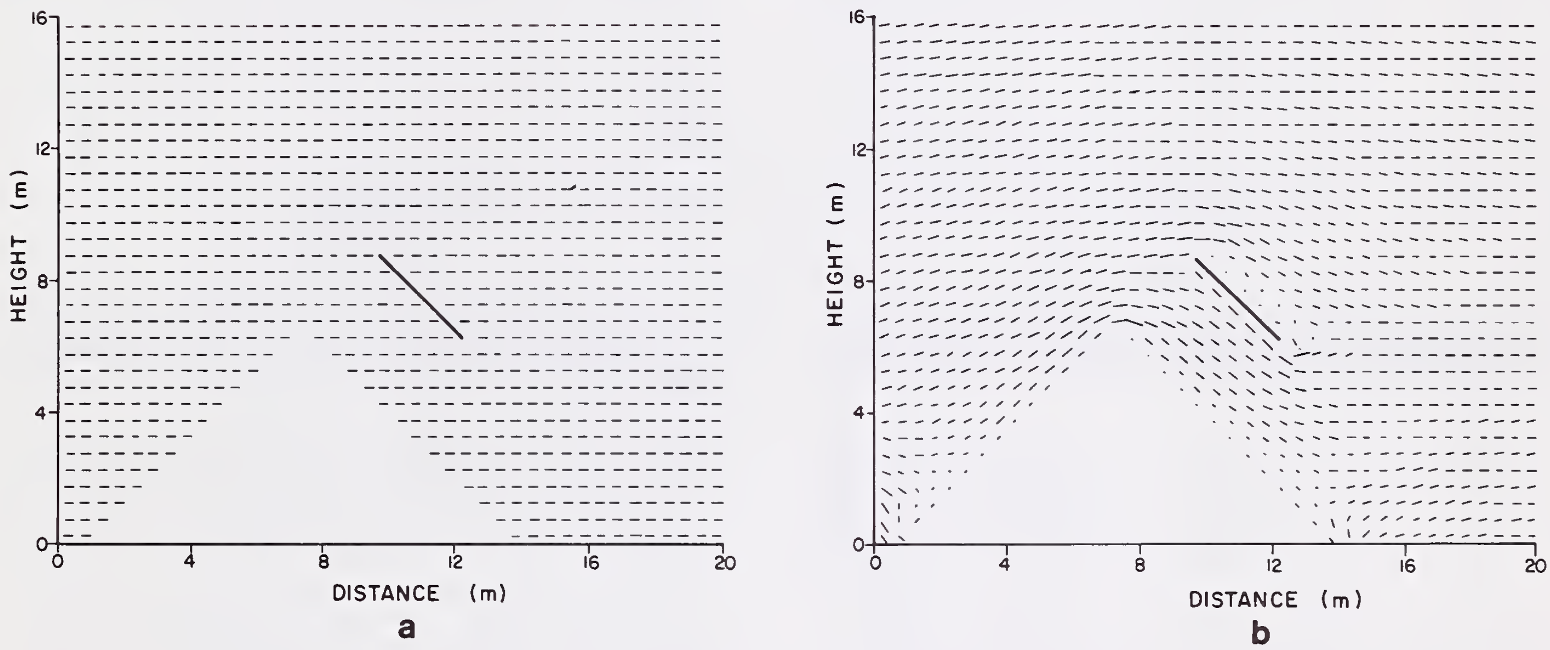

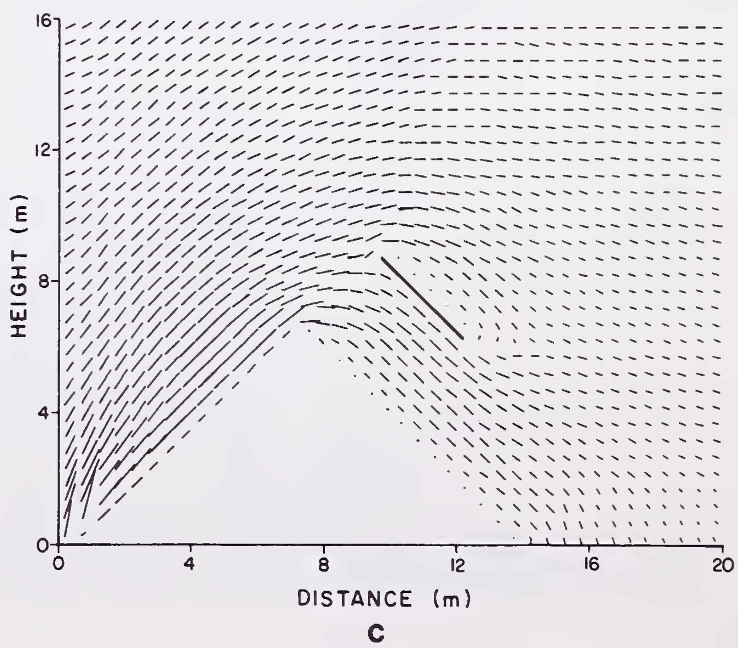

Figure 6.—Development of flow field for the full ridge model with a slope-parallel jet roof, 3.5-m characteristic length.

a. Cycle 0.
b. Cycle 1.
c. Cycle 20.

used to optimize the length and angular inclination of the jet roof. The modification involved requires a rotation of the mountain ridge through an angle within the grid such that the downwind slope is coincident with the bottom boundary of the mesh. The actual ridge crest coincides with the lower left corner of the mesh, so that only the jet roof itself is present within the grid. This final modification is shown in figure 8. For reference purposes, the development of the flow pattern in the "no-ridge model" without a jet roof is given in figure 9.

Required modifications to the SOLA-SURF code are in the sections for specifying and setting boundary conditions (2000 and 2600 sections). In the two previous models, a continuative flow boundary is specified at all boundaries, and a continuous inflow

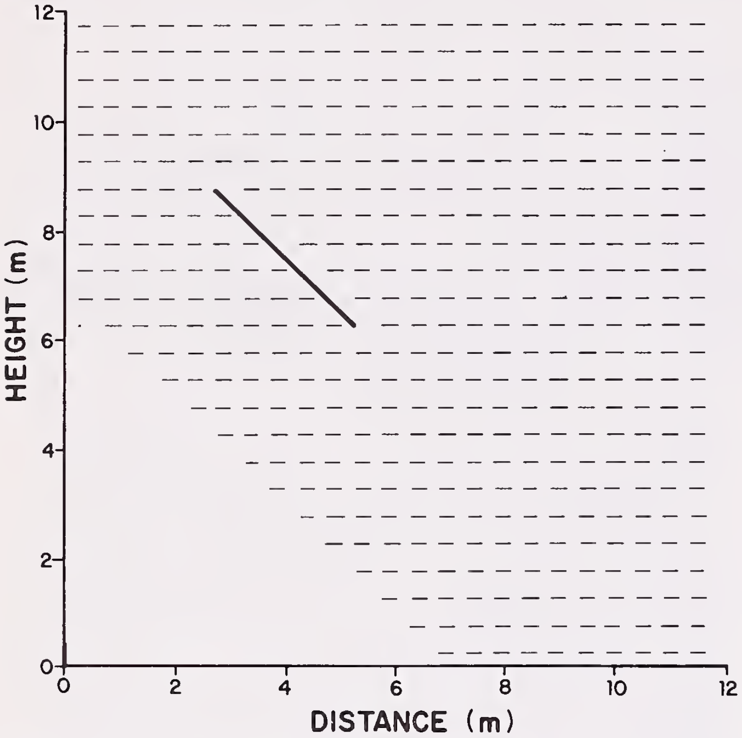

Figure 7a.—Development of flow field for the half ridge model with a slope-parallel jet roof, 3.5-m characteristic length, cycle 0.

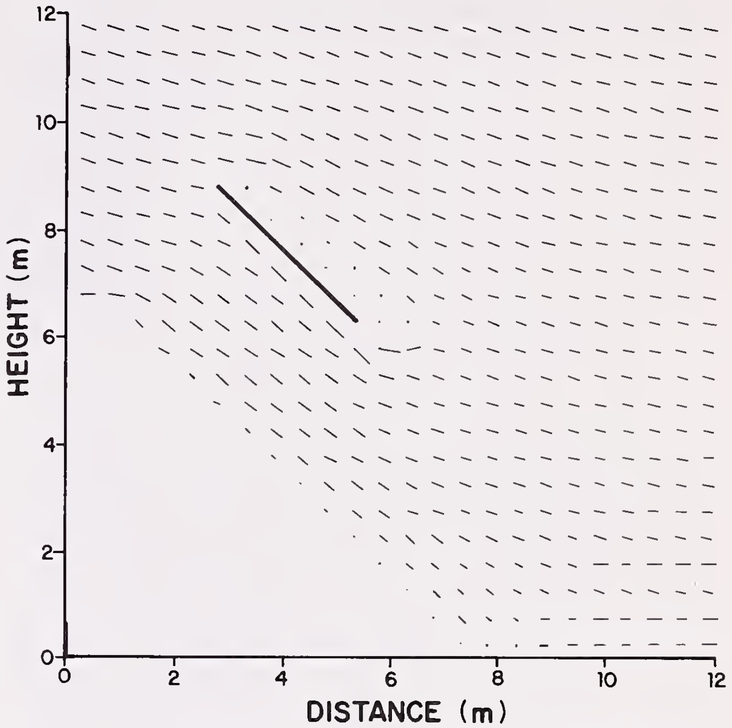

Figure 7b.—Development of flow field for the half ridge model with a slope-parallel jet roof, 3.5-m characteristic length, cycle 1.

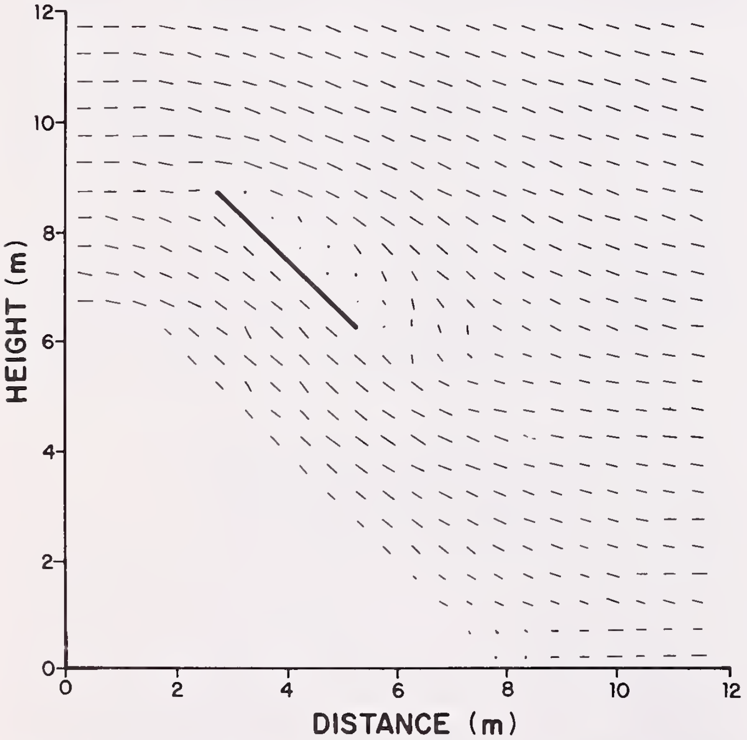

Figure 7c.—Development of flow field for the half ridge model with a slope-parallel jet roof, 3.5-m characteristic length, cycle 20.

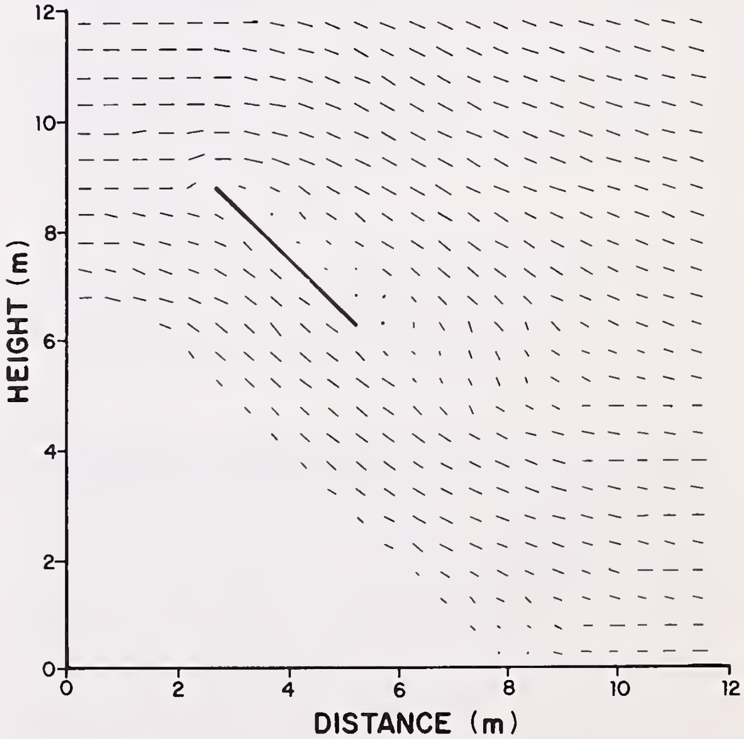

Figure 7d.—Development of flow field for the half ridge model with a slope-parallel jet roof, 3.5-m characteristic length, cycle 40.

Figure 8.—Development of flow field for the no-ridge model with a slope-parallel jet roof, 3.5-m characteristic length.
a. Cycle 0.
b. Cycle 1.
c. Cycle 20.
d. Cycle 40.
e. Cycle 60.
f. Cycle 80.
g. Cycle 100.

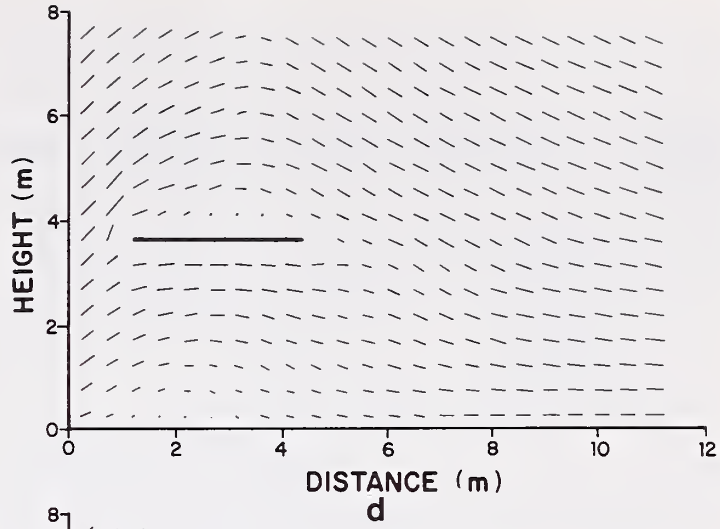

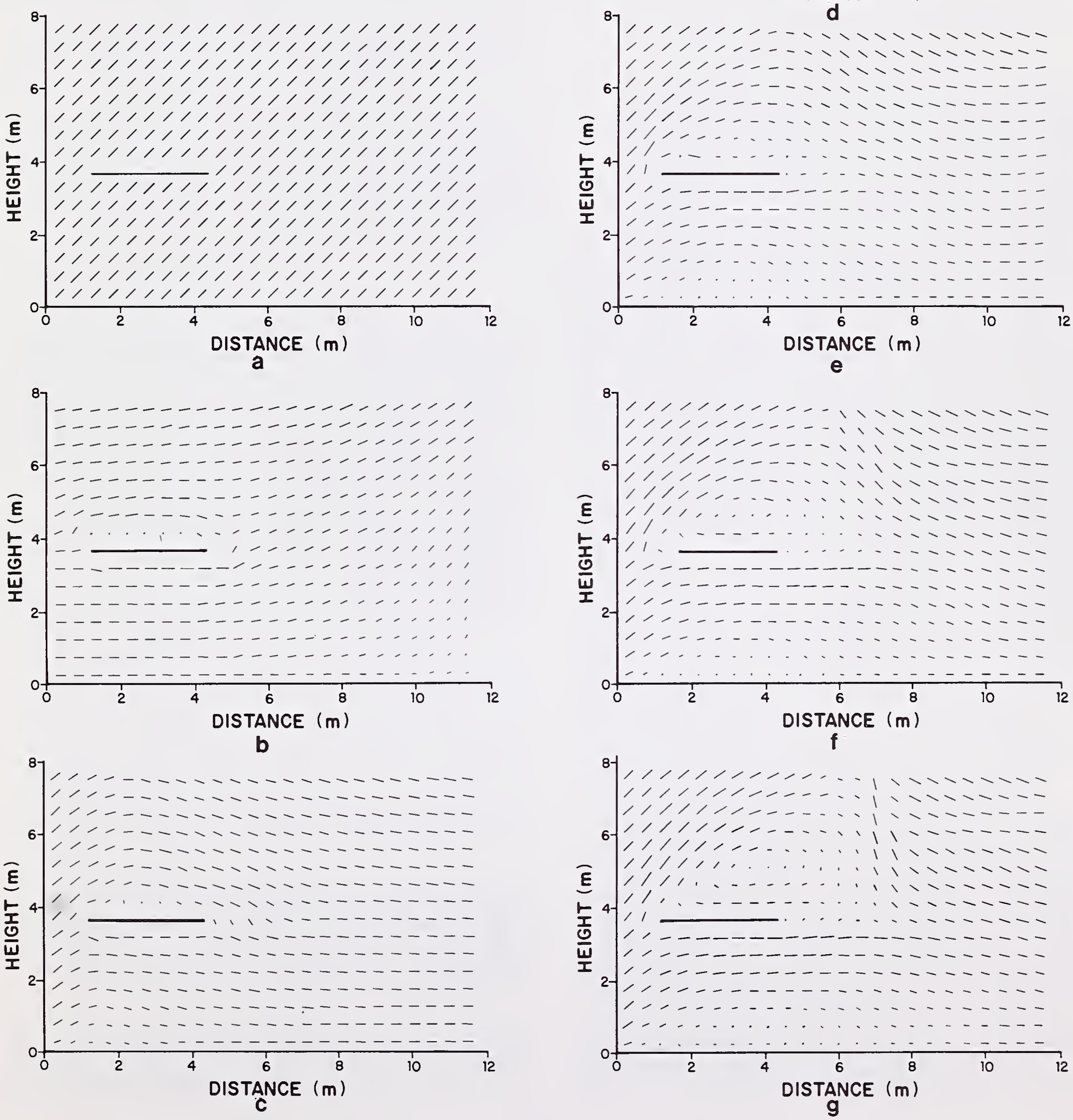

Figure 9.—Development of flow field in absence of a jet roof.
a. Cycle 0.
b. Cycle 1.
c. Cycle 20.
d. Cycle 40.
e. Cycle 60.
f. Cycle 80.
g. Cycle 100.

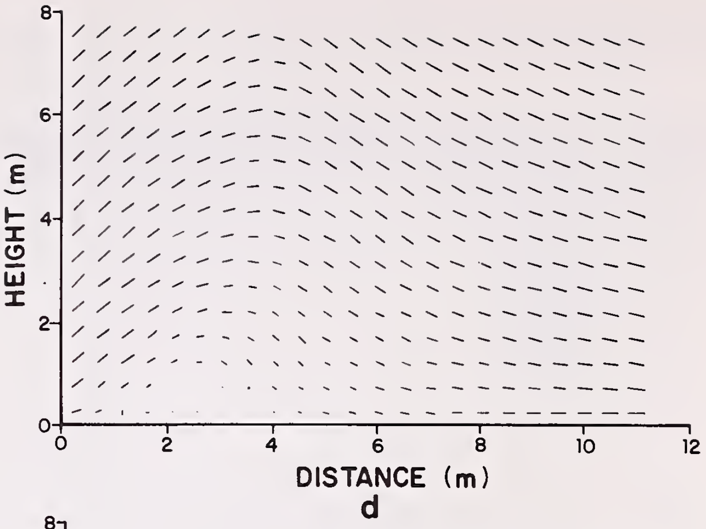

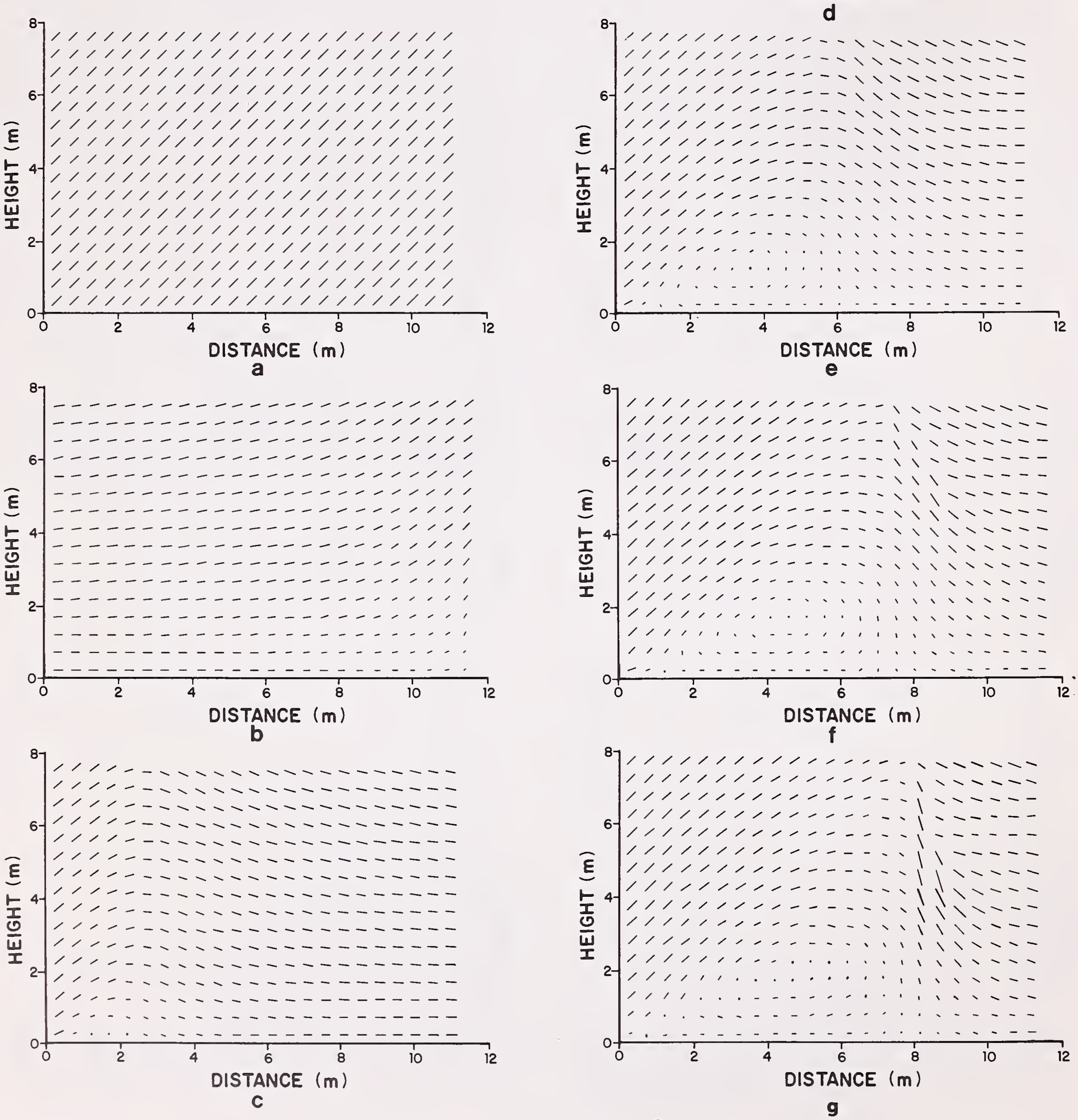

of fluid is specified along the left boundary. Whereas the full- and half-ridge peak models have only a u-component of velocity, UI, initially (VI = 0.0), and only a u-component of velocity specified in the continuous inflow condition along the left boundary, the "no-ridge" model has two components of velocity, UI and VI, specified initially along the left boundary. These velocities are functions of the angle through which the downwind slope is rotated, so that it will become coincident with the bottom of the mesh in the manner of figure 8. The primary advantages to this model are a savings in memory storage space requirements and program run-time, and the fact that we can make use of a more finely resolved grid (corresponding to selecting smaller mesh increments) for use in optimizing the angular inclination of the jet roof. A velocity vector plot showing the development of the flow is shown in figure 8.

The reason for using the modified flow model of figure 8 lies in the fact that dynamic similarity in the flows is noted between the full-, half-, and no-ridge[3] models, particularly in the location and magnitude of recirculating eddies and stagnation flow patterns.

Jet Roof Optimization

The characteristic length, angular inclination (relative to the downwind slope surface) and position on the slope of the jet roof are optimized so as to minimize the accumulation of snow in the vicinity of the jet roof and to have the greatest effect on maximizing the "scour region" along the slope.

Optimum length is that for which the least possible amount of stagnation exists underneath the roof and just beyond the trailing edge when the jet roof is parallel to the downwind slope. Stagnation occurs when the air flow comes to rest in isolated localities within the grid during the development of the flow patterns. In the areas of stagnation, a settling and resulting accumulation of snow is expected.

The development of regions of stagnation is usually noted on plots of the flow field as localized areas with low fluid velocities near the slope surface or in the form of recirculating eddies above and beyond the trailing edge of the jet roof.

The following notation is used in the JETROOF code to denote the location of the leading and trailing edge of the jet roof:

ILE = i index of the cell containing the leading edge
JLE = j index of the cell containing the leading edge
ITE = i index of the cell containing the trailing edge
JTE = j index of the cell containing the trailing edge

[3]*Printouts of the full-ridge and no-ridge models are available upon request from the USDA Forest Service, Rocky Mountain Forest and Range Experiment Station, 240 W. Prospect Street, Fort Collins, Colo. 80526.*

The first criterion of optimization establishes a relationship between the velocity gradients between the slope surface and the jet roof at the leading and trailing edges. This relationship is described physically as how the ratio of the average velocity between the slope surface and the jet roof at the leading and trailing edges is changing with respect to time. This ratio is written in terms of the leading and trailing edge velocities at some t, as

$$\mathrm{VELRA1} = \frac{\dfrac{1}{\mathrm{JLE}-2} \sum_{j=2}^{\mathrm{JLE}-1} \left[(u(\mathrm{ILE}, j))^2+(v(\mathrm{ILE}, j))^2\right]^{1/2}}{\dfrac{1}{\mathrm{JTE}-2} \sum_{j=2}^{\mathrm{JTE}-1} \left[(u(\mathrm{ITE}, j))^2+(v(\mathrm{ITE}, j))^2\right]^{1/2}} \qquad [7]$$

The development of the velocity ratio, VELRA1, as a function of time for a variety of slope-parallel jet roof lengths at a height of approximately 3.75 m above the slope surface are shown in figure 10. The plot for the 1.0-m jet roof length is the limiting case for the mesh increments selected (DELX = DELY = 0.5m). Figure 10 indicates that the flow transients under the jet roof decay rapidly at low real times. As a result the jet roof is an efficient device for control of air flows since the initial transients decay rapidly. The curves of figure 9 are generated from time and velocity ratio data computed up to cycle 100 at program termination. For exact steady-state flow prediction, computations beyond cycle 100 are necessary.

In view of the previous definition of the optimum jet roof length, the effect which the jet roof length has on the flow downslope from the trailing edge must also be considered. Figure 11 shows the development of the flow a distance downslope from the trailing edge (the "recovery distance") equal to the characteristic length of the jet roof, and indicates how the flow recovers from the effects of the jet roof at that distance. The velocity ratio, VELRA2, is plotted as a function of time, where VELRA2 is the ratio of the average velocities between the slope surface and trailing edge and at the same height at the recovery distance. The velocity ratio, VELRA2, is computed in a manner analogous to that of the first velocity ratio, VELRA1, given by equation [7].

Ideally, the transition from transient to steady flow conditions should occur in minimal time. The velocity ratio, VELRA1, should converge to a value which is relatively close to unity, which indicates approximately equal velocities at the leading and trailing edges of the jet roof. Plots of the velocity vector field show that there is a definite relationship between the velocity ratio, VELRA1, the height and position of stagnation under the jet roof, and the characteristic length of the roof. Following a similar argument, it is also desirable that the recovery distance velocity ratio, VELRA2, converge to a con-

stant value as quickly as possible after the flow begins. The steady-state value of VELRA2 should be greater than that of VELRA1, for effective scouring, but still in the vicinity of unity. This indicates a state of flow in which the velocities at the beginning of the recovery distance are somewhat greater than those at the end of the recovery distance. This condition minimizes the accumulation of snow at the trailing edge of the jet roof and effectively maintains the desired scouring action throughout the recovery distance. The velocity vector plots show that a continuous flow is present throughout the recovery distance. Considering all of these criteria, a choice of

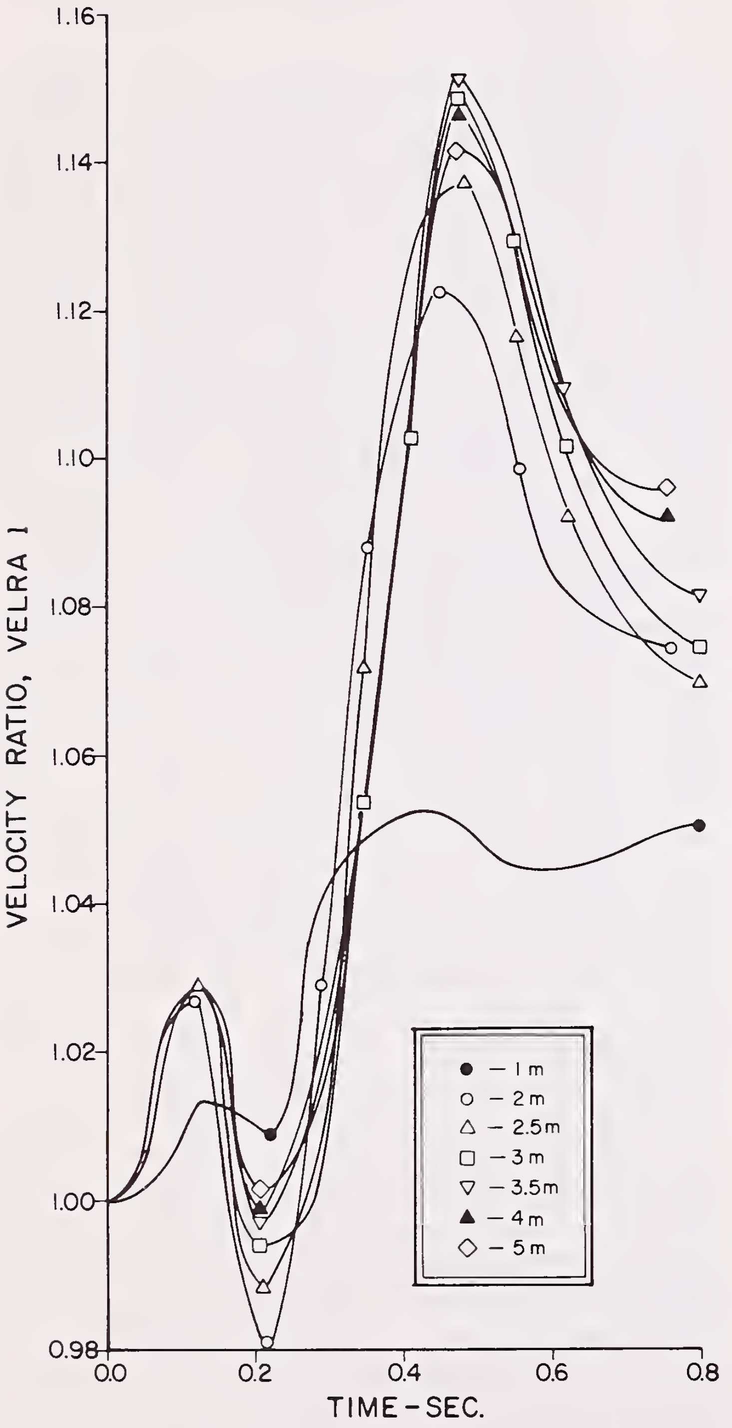

Figure 10.—Ratio of average trailing edge to recovery distance velocities for the jet roof parallel to surface.

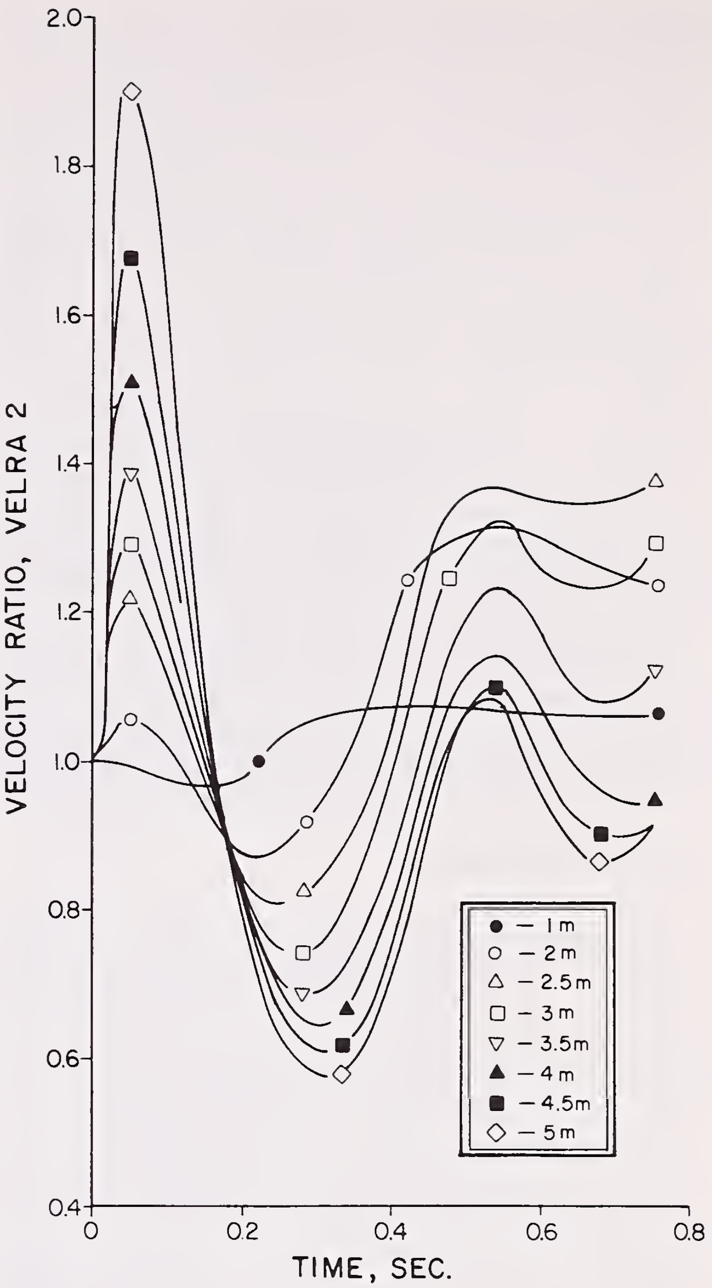

Figure 11.—Ratio of average trailing edge to recovery distance velocities for the jet roof parallel to surface.

a jet roof length of 3.0 m appears to be optimum (figs. 10, 11).

The development of the flow field for a slope-parallel jet roof 3.0 m long, as shown in figure 12, indicates a region of stagnation approximately 1.0 m high and 4.0 m long under the jet roof. A variety of runs using slope-parallel jet roofs varying in length from 1.0 m to 5.0 m show that the length of the stagnation region is less sensitive to jet roof length variations than is the height of the region. Within constraints of the finite difference model, stagnation height can be reduced by positioning the jet roof closer to the surface.

In initial studies using coarser mesh increments of DELX = DELY = 1.0 m, the stagnation under the jet roof could be eliminated by positioning the roof closer to the surface. However, this does not represent the true physical situation for two reasons. First,

most jet roofs now in use are situated parallel to the downwind slope and from 2.44 to 4.27 m above the slope (Montagne et al. 1968). Second, when coarse mesh increments are used, a serious loss of spatial resolution and computational accuracy is noted as the jet roof is moved closer to the slope surface. As fewer cells are maintained between the slope surface and the jet roof, the flow under the roof is forced to assume a nonrotational pattern since there is only one set of spatial variables (two components of velocity and one pressure) per cell.

Consider next the effect that inclining the jet roof has on reducing stagnation under the roof, and on scouring the downslope region. The angular inclination of the jet roof relative to the slope surface is optimized in a manner similar to that of determining the optimum jet roof length. The optimum jet roof inclination is the angular inclination relative to the surface of the downwind slope, which has the greatest effect on reducing the height and length of the region of stagnation.

The inclination of the jet roof is handled as shown in figure 13, in which the velocities of the corresponding cells are set equal to zero. Figure 13 shows a jet roof inclination of $\Phi = -9.5°$ relative to the downwind slope surface. A number of jet roof inclinations were considered including Φ = -45°, -22.6°, -9.5°, -4.8°, 4.8°, 9.5°, 22.6°, and 45°. The values of VELRA1 and VELRA2 are plotted for increasing time in figures 14 and 15 in a manner similar to that for the parallel jet roof in figures 10 and 11, respectively.

Ideally, the velocity ratio plots of figures 14 and 15 for the inclined jet roof will exhibit characteristics similar to those desirable for the slope-parallel jet roof. It is also important to consider the velocity vector plots showing the development of the flow field for jet roofs of both positive and negative inclinations. Jet roofs with negative inclinations (inclined downward) have a pronounced effect in reducing the stagnation under the jet roof. Jet roof inclinations which are positive (inclined upward) result in an increased stagnation near the surface toward the trailing edge of the roof. Therefore, an undesirable deposition of snow can be expected to occur in this area. Thus, the jet roof should be inclined downward to have the greatest effect in reducing stagnation under the jet roof and to allow the flow to return to its normal pattern as soon as possible after passing the jet roof.

Additionally, as noted from the velocity vector plots, any inclination of the jet roof causes a large recirculating eddy to be formed just above its trailing edge. As the angle of inclination increases, so does the size of the recirculating eddy. The presence of this recirculating eddy tends to cause two problems. First, snow may be deposited on the trailing edge of the jet roof which will load the structure and change the flow characteristics. Second, the possibility exists of an accumulation further downslope that the flow next to the surface can not eliminate. This snow accumulation is not indicated on the velocity vector plots for the inclined jet roofs examined, but was noted by Montagne et al. 1968 in field experiments using jet roofs erected to control cornice development in the Bridger Range of southwestern Montana.

Using the above discussion as a guideline and considering the velocity ratio plots of figures 14 and 15 and the velocity vector plots for the jet roofs of 3.0 m length and inclined at angles of Φ = -4.8°, -9.5°, -22.6°, -45°, 4.8°, 9.5°, 22.6°, and 45°, respectively, a jet roof which is inclined at an angle of $\Phi = -9.5°$ was selected as the optimized design for which the stagnation region and the recirculating eddy above the trailing edge are both minimal. The development of the flow field for the optimized jet roof (jet roof length = 3.0 m, $\Phi = 9.5°$) is shown in figure 16.

Final consideration is given to placement of the jet roof relative to the ridge of the mountain. Using a jet roof configuration of length 3.0 m and relative slope angle to the lee slope of $\Phi = 0°$, consider four positions of the roof. The four configurations are indicated in figures 17a,b,c,d and will be designated as Cases A,B,C,D, respectively, in the following discussions. The quasi-steady-state flow patterns shown in figure 17 qualitatively depict the properties of the four geometric cases, in which trends in the recirculation and stagnation regions can be defined. To further appraise these cases, the average velocity at the trailing edge of the jet roof, and the volume flow rate per unit width of jet roof are computed and summarized in table 1.

Table 1.—Average velocity and volume flow rate at the vertical cross section at the trailing edge of the jet roof

Case	Average Velocity (m/s)	Volume Flow Rate (m^3/s)
A	13.9	48.8
B	18.6	43.3
C	19.9	30.4
D	20.2	15.9

The low average velocity of Case A is one design condition that is conducive to jet roof jamming by excessive snow deposition. In Case D, a second design condition is exemplified of low volume flow rate, a condition for limited scour region effectiveness. Excluding these cases, Cases B and C remain, for which further evaluation is considered in the conclusions section.

Figure 12.—Development of flow field for optimum slope-parallel jet roof, 3.0-m characteristic length.
- a. Cycle 0.
- b. Cycle 1.
- c. Cycle 20.
- d. Cycle 40.
- e. Cycle 60.
- f. Cycle 80.
- g. Cycle 100.

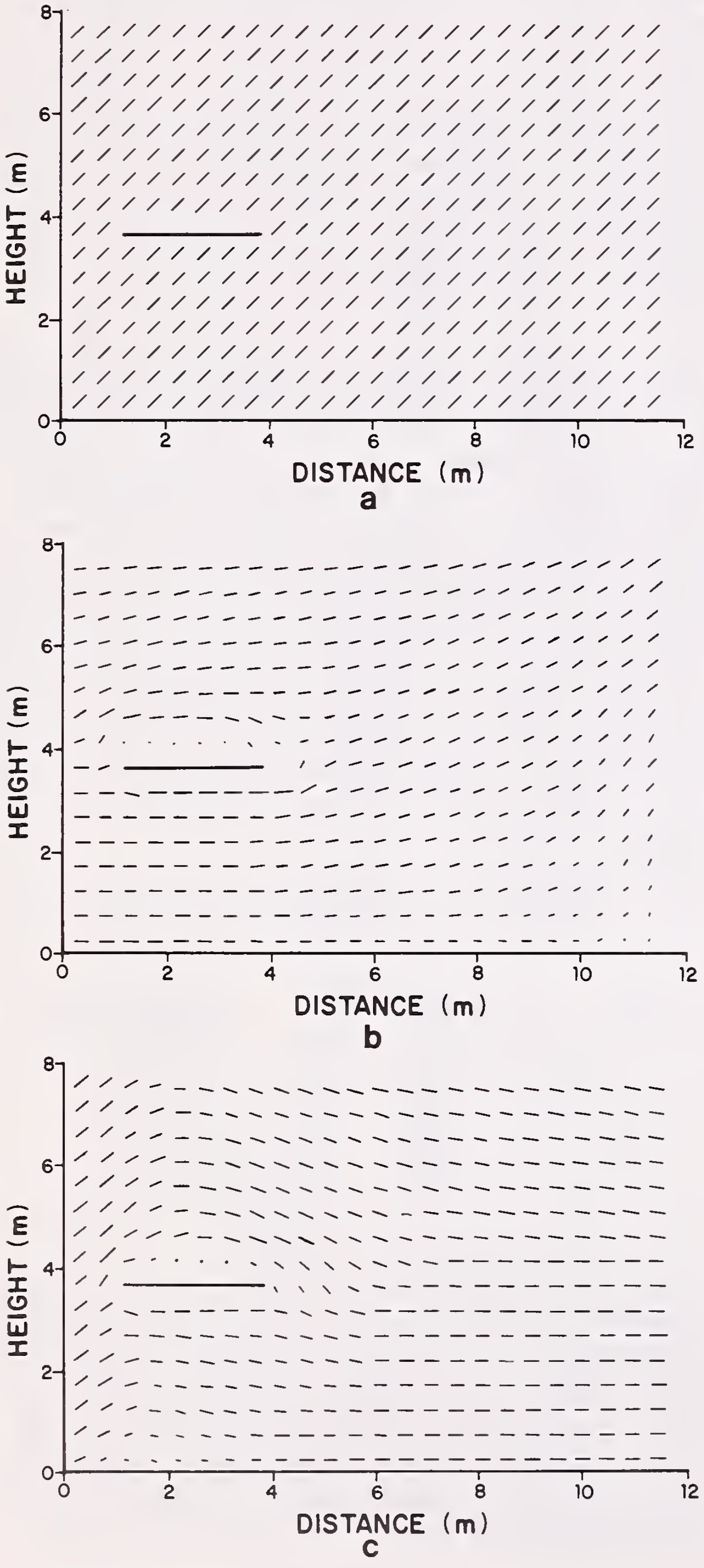

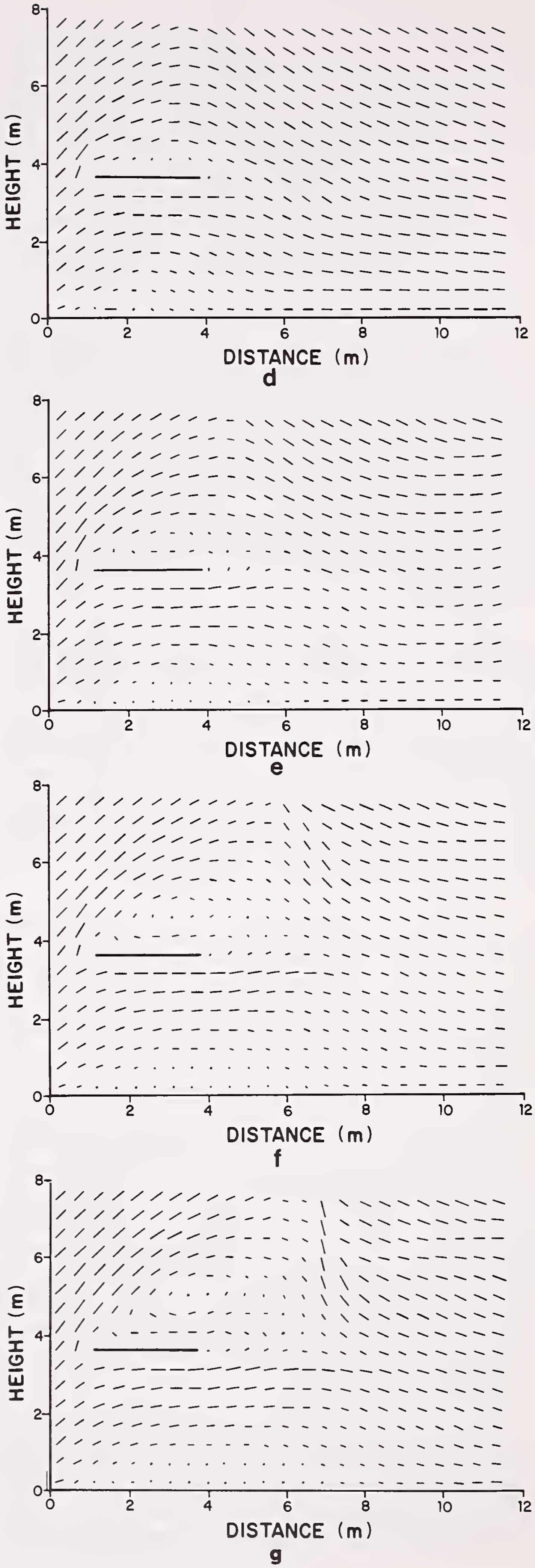

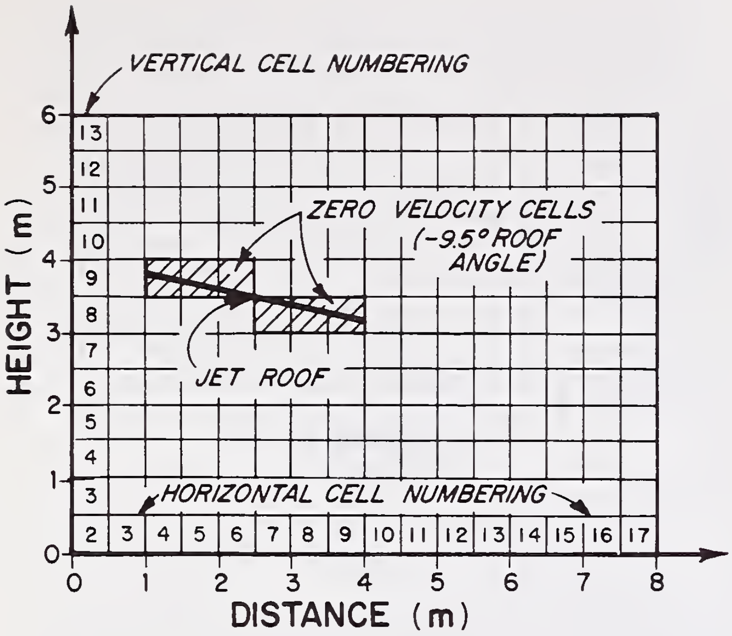

Figure 13.—Jet roof with location of cells for finite difference approximation of jet roof inclination relative to mean slope surface $\phi=-9.5°$.

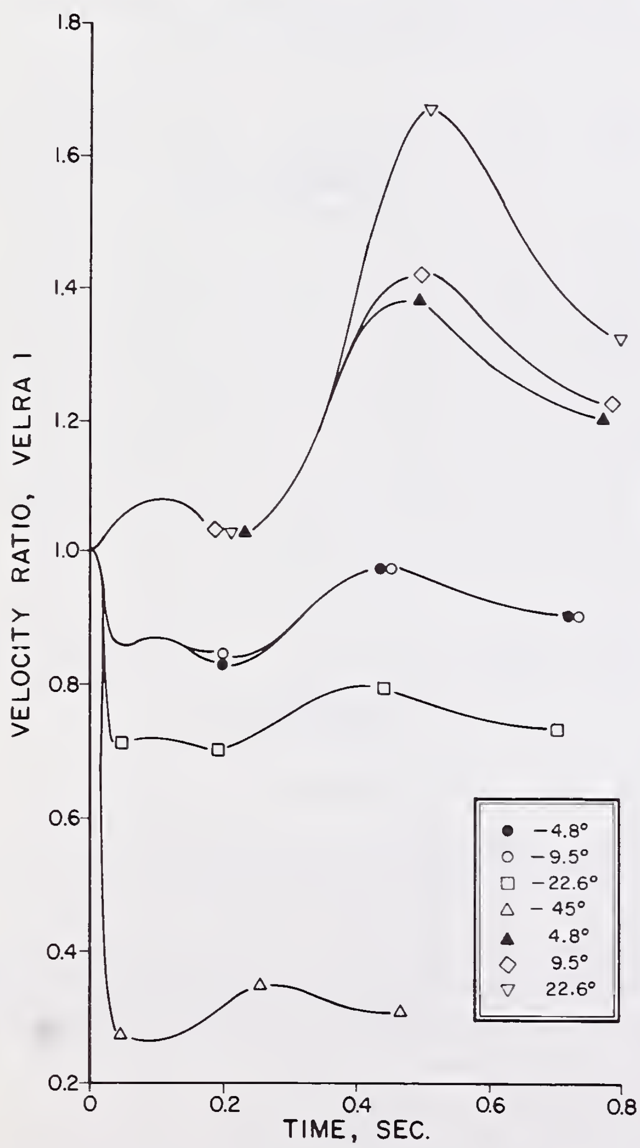

Figure 14.—Ratio of average leading to trailing edge velocities for the jet roof inclined relative to surface, jet roof length = 3.0 meters.

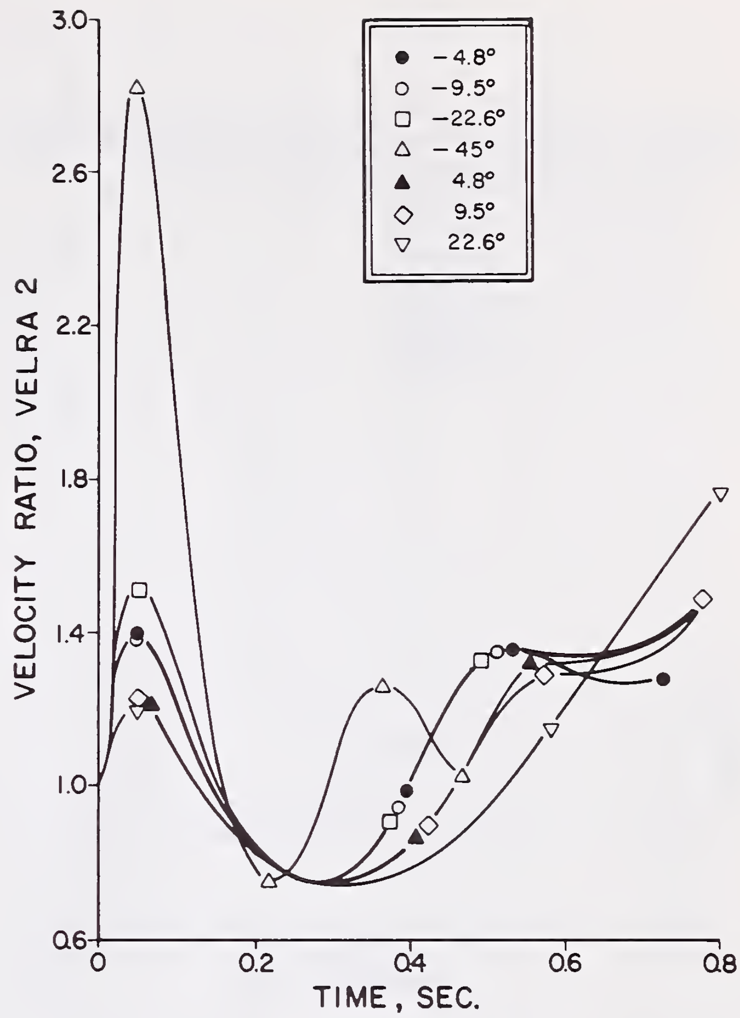

Figure 15.—Ratio of average trailing edge to recovery distance velocities for the jet roof inclined relative to surface, jet roof length = 3.0 meters.

Output data and velocity vector plots for slope-parallel and roof-angle cases not reported herein are reported in a supplemental document that lists these data.[4]

Certain conditions on numerical stability relate to all the jet roof models that have been evaluated. Referring to figure 17, the bottom boundary of the computational grid is specified as a slip-free rigid boundary. In earlier runs with the full-ridge and half-ridge models, a continuative inflow-outflow boundary was specified at the bottom, which did not affect the flow pattern at the jet roof, but resulted in a greater number of iterations for each cycle. Another numerical instability results when the number of cells vertically above the jet roof is reduced to one or two instead of five or more. For, say, two cells above the roof, the recirculation condition may result in adjacent cells having large equal and opposite vertical velocities, which lead to a rapidly developing numerical instability. This condition is eliminated in

[4]Dawson, K.L. and T.E. Lang. "Listings of flow field plots from numerical simulation of air flow past jet roof geometries for snow cornice control," USDA Forest Service, Rocky Mountain Forest and Range Experiment Station, Fort Collins, Colo. 80526 (on file).

Figure 16.—Development of flow field for optimum sloping jet roof, 3.0-m characteristic length, Φ = -9.5°.

a.	Cycle 0.
b.	Cycle 1.
c.	Cycle 20.
d.	Cycle 40.
e.	Cycle 60.
f.	Cycle 80.
g.	Cycle 100.

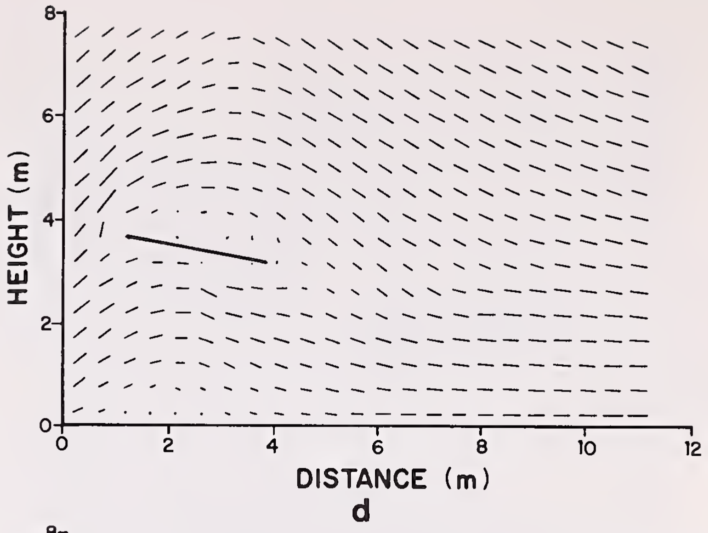

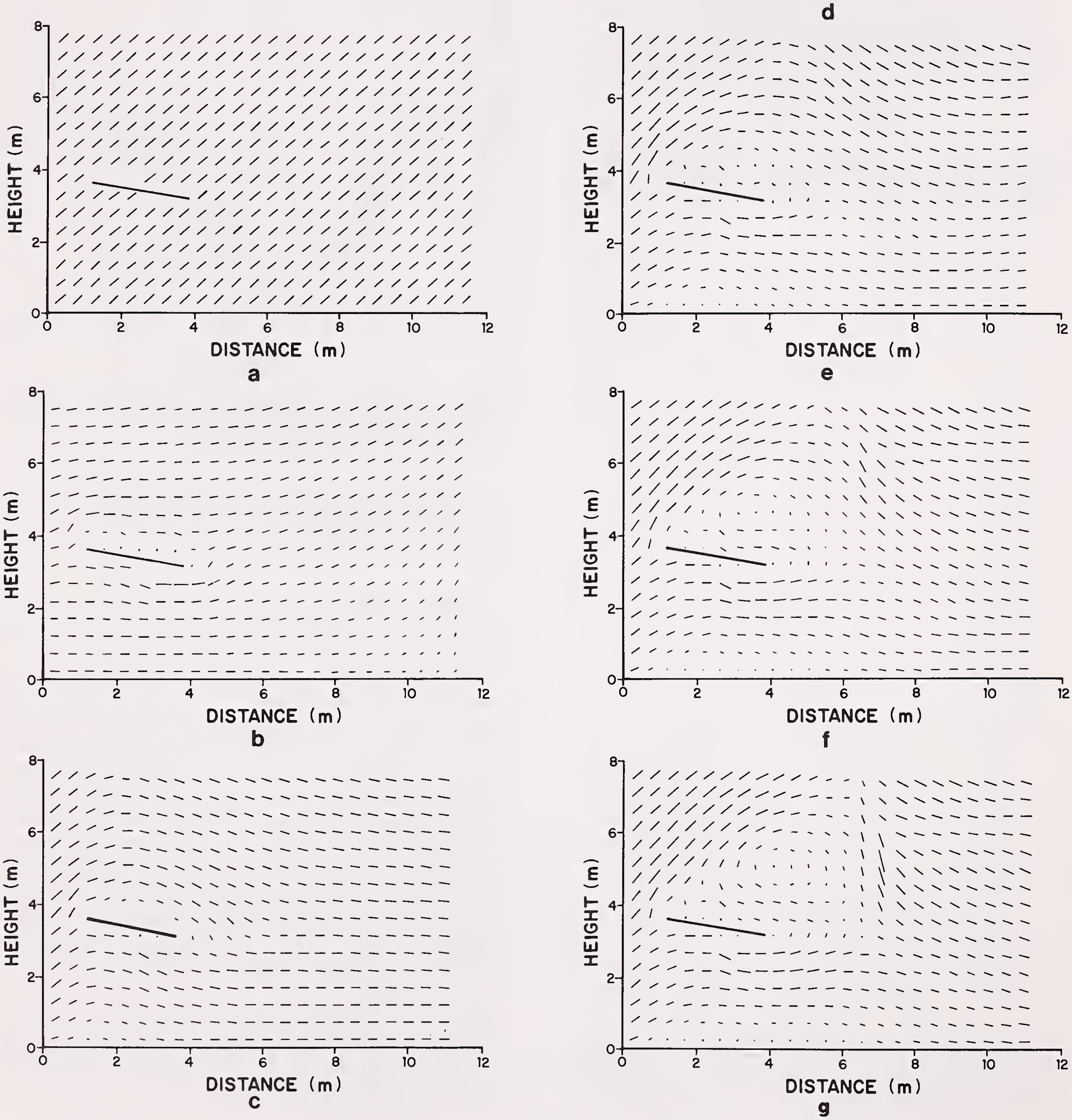

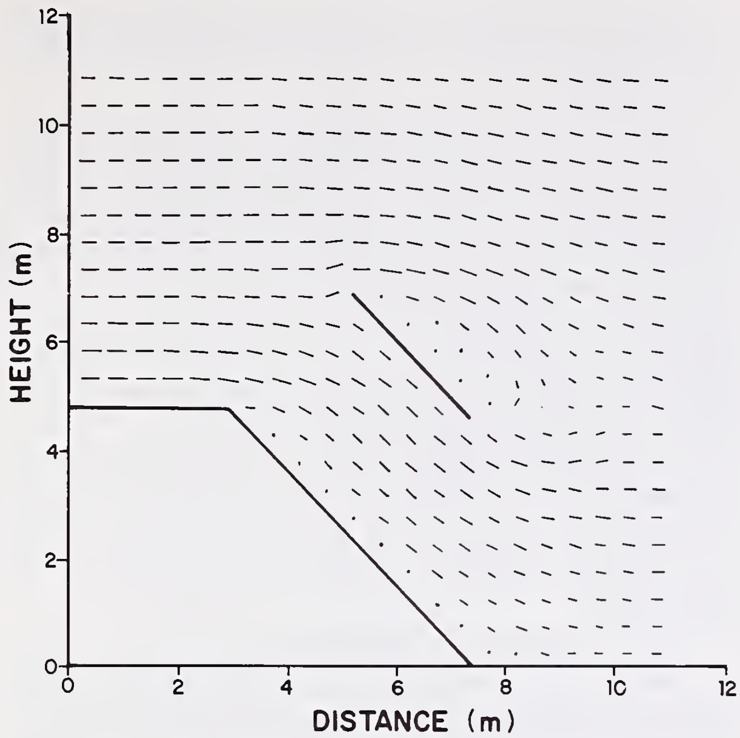

Figure 17a.—SOLA-SURF jet roof with vorticity flow mountain ridge flow, Case A.

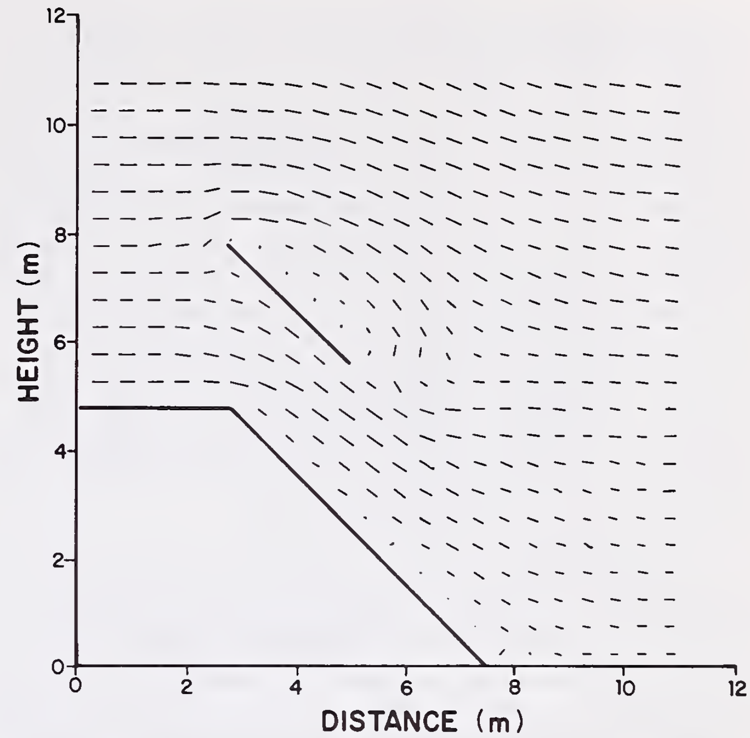

Figure 17b.—SOLA-SURF jet roof with vorticity flow mountain ridge flow, Case B.

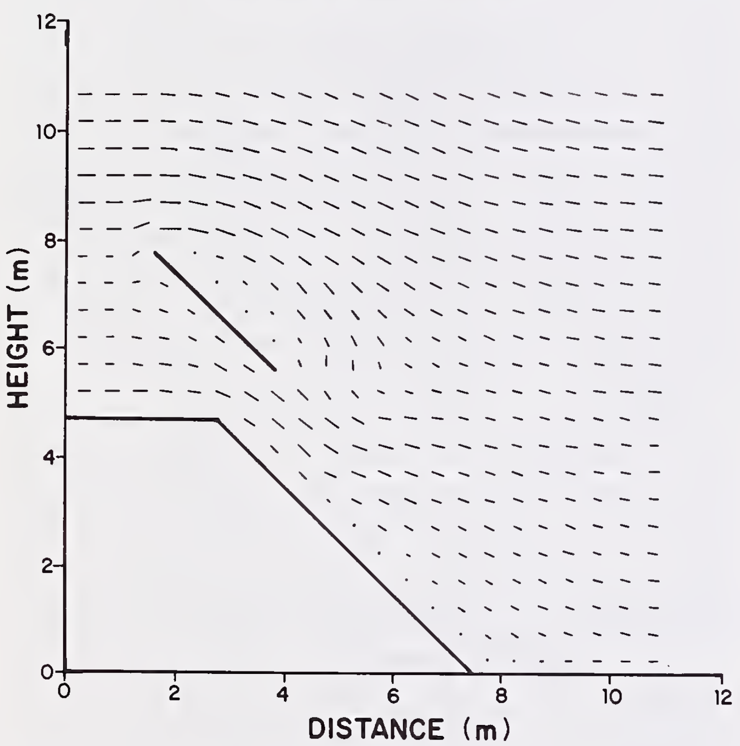

Figure 17c.—SOLA-SURF jet roof with vorticity flow mountain ridge flow, Case C.

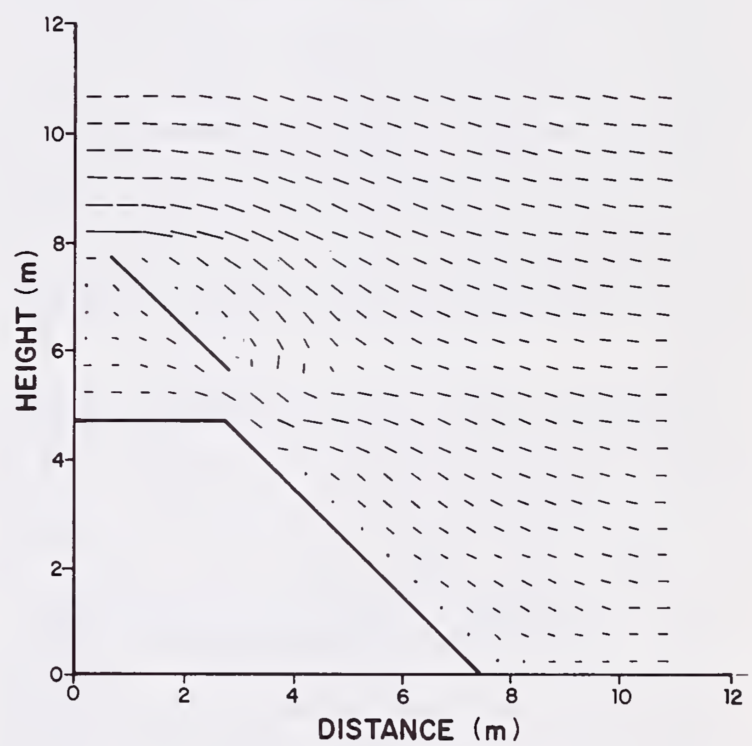

Figure 17d.—SOLA-SURF jet roof with vorticity flow mountain ridge flow, Case D.

expanding the domain so that five or more cells are used above the jet roof, depending upon the vertical extent of the recirculation region.

Conclusions

The use of a jet roof as a flow spoiling device can be a valuable asset in controlling the development of snow cornices (Montagne 1968). For a particular ridge geometry, prevailing winds, and fixed roof height, primary variables are the roof length, angular inclination, and roof orientation relative to the ridge in controlling stagnation region and recirculating eddy developments.

The three mathematical models, designated the full-ridge, half-ridge, and no-ridge models, are found to equally represent air flow past a jet roof on the downwind side of a ridge. The no-ridge version is a

valid simplification of the other two models as a result of the dynamic similarity of the flow fields between each model. The no-ridge model also represents the most efficient and economic use of the JETROOF code. Additionally, the successive simplifications to the no-ridge model without disturbance to the flow field past the jet roof implies negligible dependence of the flow pattern on upwind geometry of the mountain. Thus, the results obtained are general for any upwind mountain geometry that does not exclude the jet roof from being considered as placed at a ridge. Turbulence, which is likely to be present in actual air flow at a ridge, is considered a secondary effect for steadiness of the flow in defining scour region and stagnation zones.

Considering the plots of the developing flow fields for both the slope-parallel (fig. 12) and inclined (fig. 16) jet roof, note that the characteristic length of the jet roof controls the height of the stagnation region. In contrast, the inclination of the roof controls the length, height and position of the stagnation region. These results are further verified in the summary plots of figures 18, 19, and 20 which show the basic stagnation and eddy regions for the different geometric configurations that have been evaluated. Figure 18 shows the changes as a function of jet roof length for the slope-parallel case. Figures 19 and 20 show the changes as a function of the angular inclination of the 3.0 m length jet roof. It is concluded that changing the length of the jet roof has little effect on the size of the stagnation region, and that angular inclination must be included in any design consideration.

Additionally, the velocity vector plots showing the developing flow fields without a jet roof present indicate that a large clockwise recirculating eddy is formed just downslope from the ridge (fig. 9). When a jet roof is introduced, the recirculation is located just above the trailing edge of the roof. The characteristic length of the jet roof affects the location of the recirculaton, whereas the angular inclination controls its size (compare figs. 18, 19, and 20). It is desirable to minimize the size of the recirculating eddy because of the possibility of deposition of snow on the trailing edge of the jet roof. Figure 20 indicates that any positive inclination of the jet roof is undesirable because it results in the formation of an enlarged stagnation region under the roof. Conversely, a negative inclination of the jet roof has a pronounced effect on reducing the stagnation under the roof (fig. 19).

An inclination angle of $\Phi = -45°$ (fig. 19) results in the smallest stagnation region of the jet roofs considered; however, the recirculating eddy is exceedingly large. It is concluded then, from the flow field plots for the inclined jet roof, that the slope-parallel jetroof or one with a small negative inclination ($-10° \leqslant \Phi \leqslant 0$) is the most efficient jet roof with respect to minimizing both the stagnation region and the recirculation.

With regard to the position of the jet roof relative to the mountain ridge, four configurations that are evaluated are shown in figure 21a and designated as Cases A,B,C,D. The developed flow fields for each of these cases are shown in figures 17a, b, c, d. The recirculation regions and the starting fronts of the stagnation regions for the four cases are shown in figure 21b. The recirculation regions show a trend toward smaller regions from Case A to Case D; however, this variation is not considered significant in selecting one configuration over another. From the standpoint of wanting the stagnation region to start as far down slope as possible, Cases B and C are preferred.

From results on average flow and volume flow rate in table 1, it is determined that although the average velocity for Case B is 7% lower than that of Case C, the volume flow rate for Case B is 33% greater than that of Case C. The greater flow rate for Case B is principally a function of the greater area of the opening at the trailing edge of the jet roof, which provides greater margin against possible snow blockage under the jet roof. In accounting for all aspects of the jet roof configurations evaluated, Case B, for which the leading edge of the jet roof is directly above the mountain ridge, has characteristics most desirable from a design standpoint. Since most jet roof configurations tested to date have been oriented as in Case D (Perla and Martinelli 1976), further experimental verification of the Case B configuration is warranted.

Based on the observation that the jet roof can control transients in the fluid flow over short time durations, long duration computer simulations are not necessary to accurately represent the state of the flow field as it approaches steady-state conditions. This would not be true in the case of mountain ridge flow models which consider the more realistic condition of variable input flow boundary conditions corresponding to wind fluctuations. This case can be modeled using the JETROOF code, wherein the input velocities at the entrance to the flow domain at the left boundary will change with respect to time, and consequently, produce a continuing transient state; however, the computer cost of this refinement is not presently justifiable.

The mesh increments DELX and DELY are user-specified parameters which control the spatial resolution of the finite difference grid, the program run time, and the accuracy of the results. The spatial resolution is an important consideration relative to the ability of the JETROOF program to detect regions of stagnation and recirculation. A coarsely resolved flow domain will reveal regions of stagnation as well

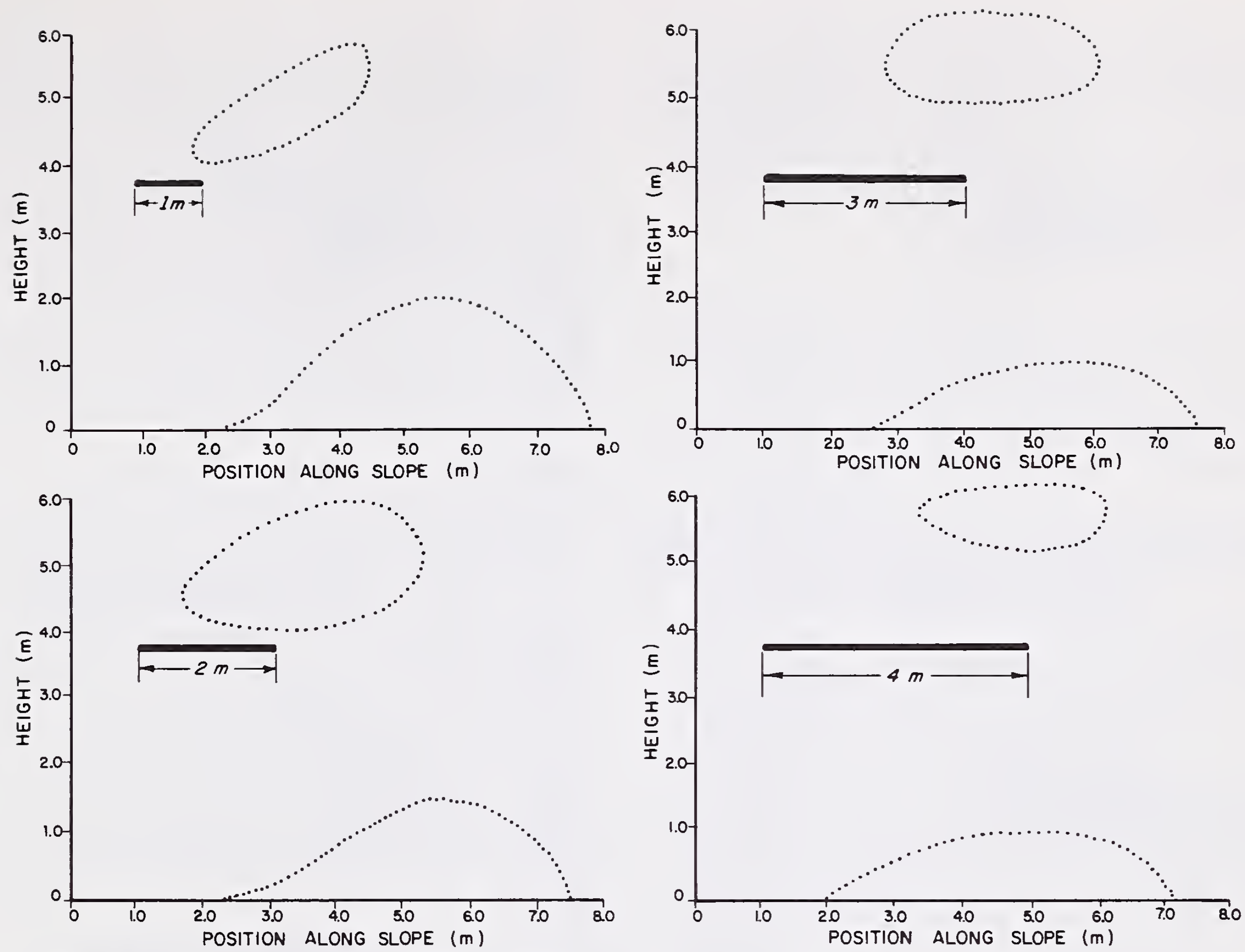

Figure 18.—Dependence of stagnation region and recirculaton eddy upon slope-parallel jet roof.

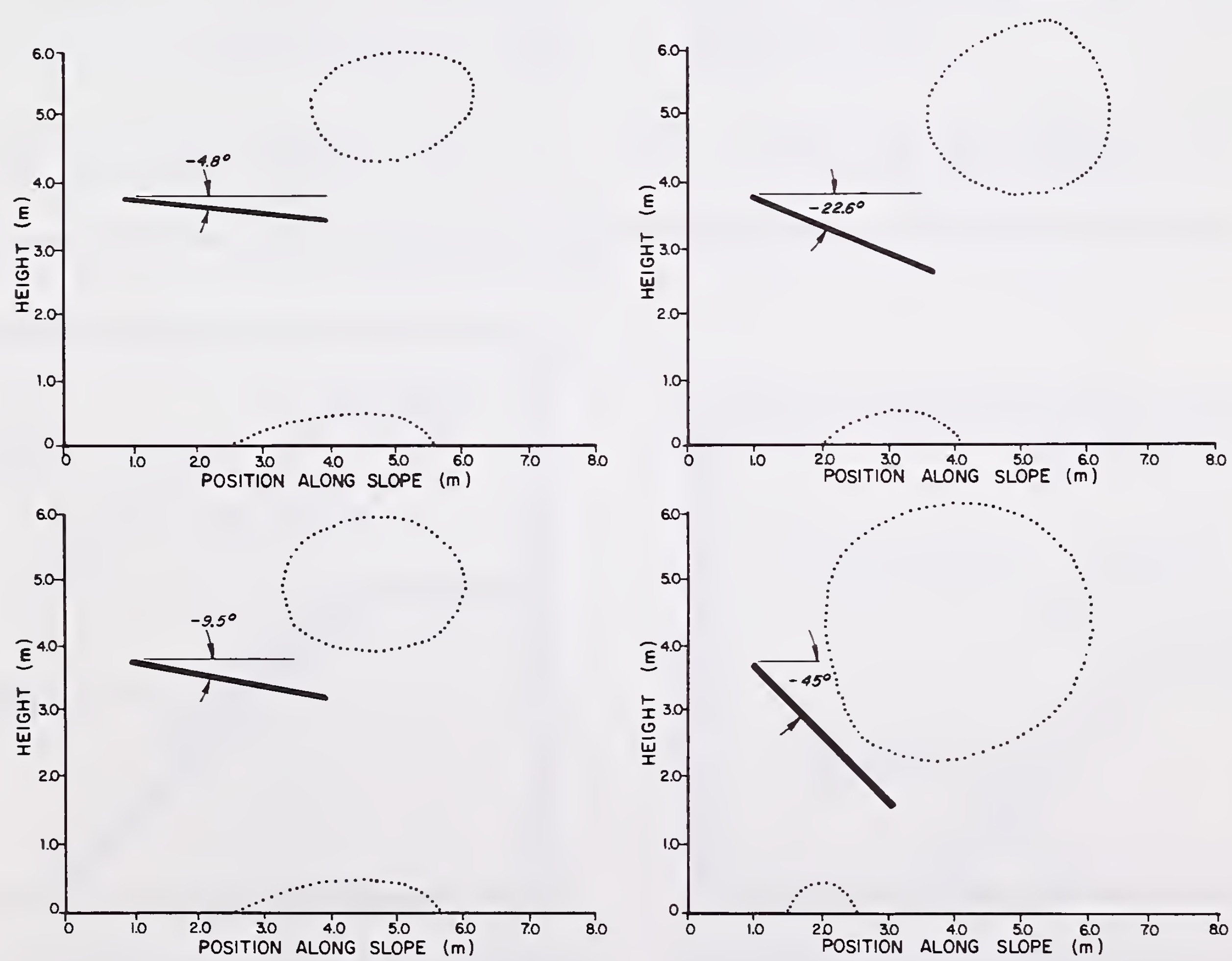

Figure 19.—Dependence of stagnation region and recirculation eddy upon negative jet roof inclination for a jet roof 3.0 m long.

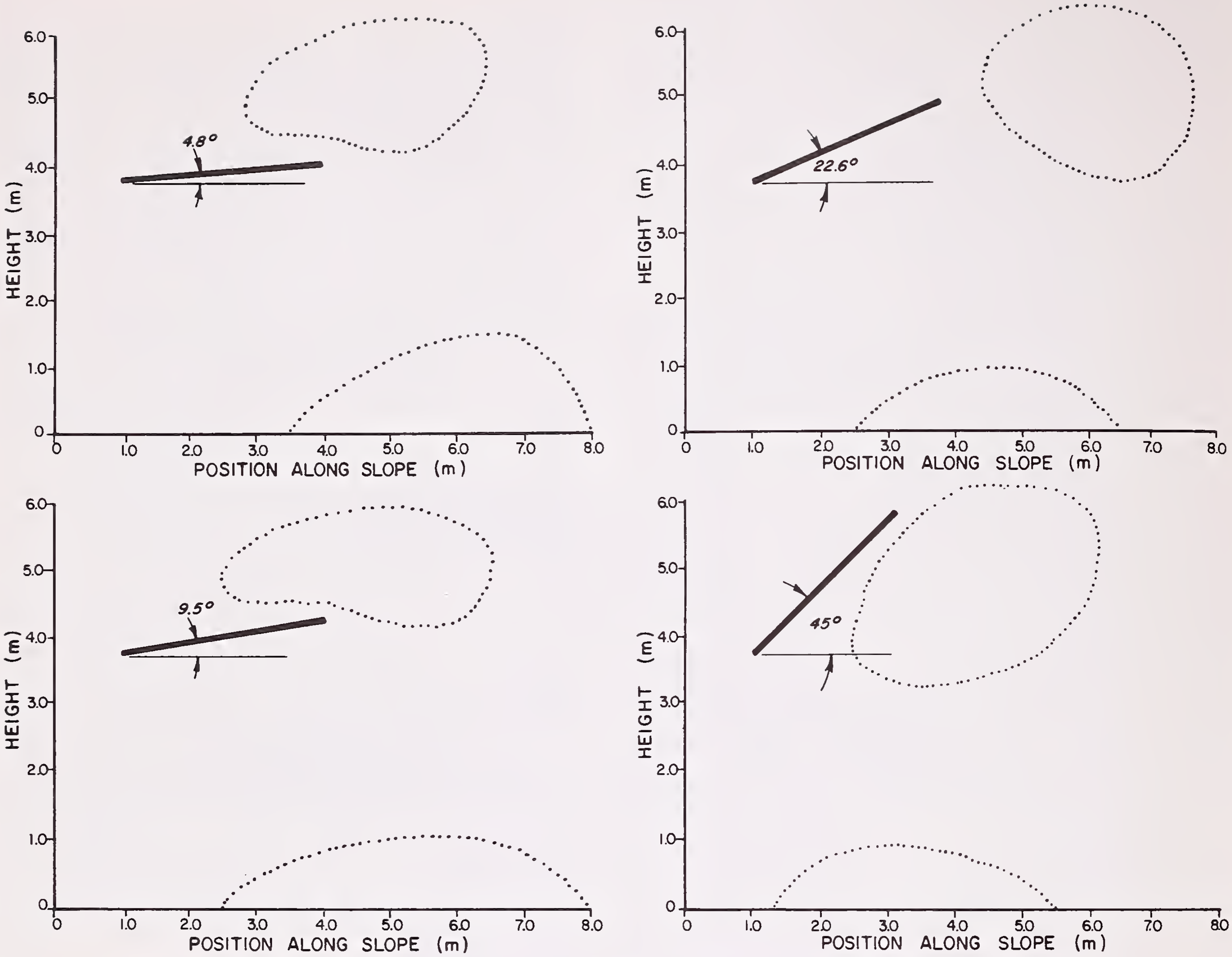

Figure 20.—Dependence of stagnation region and recirculation eddy upon positive jet roof inclination for a jet roof 3.0 m long.

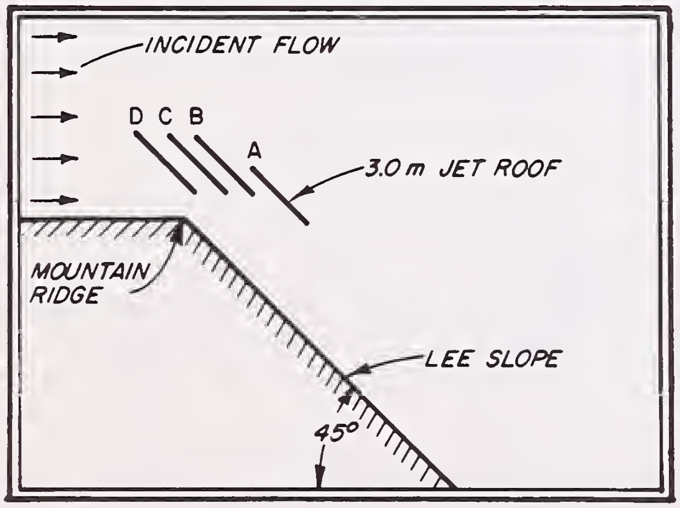

Figure 21a.—Definition of four jet roof geometries relative to the mountain ridge.

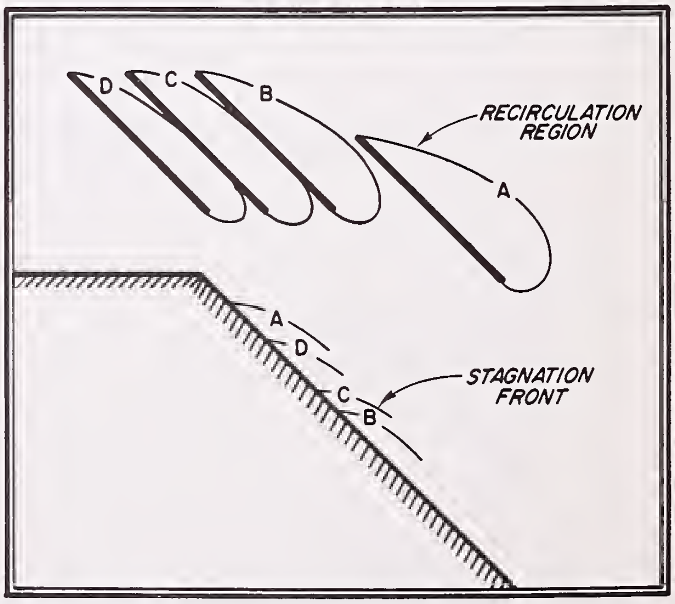

Figure 21b.—Stagnation regions and recirculation eddies for the four regions.

as a more finely resolved grid. The number of cells separating the jet roof and the ground surface should be great enough to accurately indicate the height of the stagnation region under the roof. Initial runs using a three- or four-cell separation (DELY = 1.0 m) did not correctly predict the stagnation which was shown to exist using a seven- or eight-cell separation (DELY = 0.5 m). It is concluded that a seven- to ten-cell separation between the jet roof and the ground surface provides a sufficient spatial resolution so that regions of stagnation under the roof will be correctly predicted.

Care must be exercised in using the continuative boundary condition for the upper boundary due to instabilities which may occur. The computational mesh must be of sufficient size to allow for any recirculation patterns to be detected. As the magnitude of the recirculating eddy increases, so must the height of the finite difference grid. Due to the boundary condition problems encountered as discussed earlier, the continuative boundary conditions used in the JETROOF code are difficult to satisfy when a recirculating flow containing diametrically opposed components of velocity in adjacent cells is present next to the boundary.

Program Availability

Printouts of the following computer programs for use with FORTRAN compilers are on file at the USDA Forest Service, Rocky Mountain Forest and Range Experiment Station, 240 West Prospect Street, Fort Collins, Colo. 80526.

A . Full mountain ridge and jet roof model.

B . No mountain ridge and jet roof model.

Literature Cited

Harlow, F.H., J.E. Welch, J.P. Shannon and B.J. Daly. 1966. The MAC method: A computing technique for solving viscuous, incompressible transient fluid-flow problem involving free surfaces. Los Alamos Sci. Lab., Los Alamos, N. Mex., LA 3425. 50 p.

Hirt, C.W. 1968. Heuristic stability theory for finite-difference equations. J. Comput. Phys., Vol. 2, p. 339-355.

Hirt, C.W., B.D. Nichols, N.C. Romero. 1975. SOLA: A numerical solution algorithm for transient fluid flows. Los Alamos Sci. Lab., Los Alamos, N. Mex., LA 5852. 50 p.

Montagne, John, J.T. McPartland, A.B. Super, and H.W. Townes. 1968. The nature and control of snow cornices on the Bridger Range, southwestern Montana. USDA For. Serv., Wasatch Nat. For. Alta Avalanche Stud. Cent., Misc. Rep. No. 14. 14 p.

Perla, Ronald I. and M. Martinelli, Jr. 1976. Avalanche Handbook, U.S. Dep. Agric., Agric. Handb. 489. 238 p.

Dawson, K. L., and T. E. Lang. 1978. Numerical simulation of jet roof geometry for snow cornice control. USDA For. Serv. Res. Pap. RM-206, 19 p. Rocky Mt. For. and Range Exp. Stn., Fort Collins, Colo. 80526.

A numerical solution algorithm is used to study the air flow over a mountain ridge with and without a jet roof located near the ridge crest. For the simple ridge geometry studied the roof should be parallel to the lee slope, the leading edge of the roof should be at or near the ridge crest, and the height of the leading edge above ground should be about the same dimension as the roof length from leading edge to trailing edge.

Keywords: Avalanche control, mountain snow, jet roofs, cornice control.

Dawson, K. L., and T. E. Lang. 1978. Numerical simulation of jet roof geometry for snow cornice control. USDA For. Serv. Res. Pap. RM-206, 19 p. Rocky Mt. For. and Range Exp. Stn., Fort Collins, Colo. 80526.

A numerical solution algorithm is used to study the air flow over a mountain ridge with and without a jet roof located near the ridge crest. For the simple ridge geometry studied the roof should be parallel to the lee slope, the leading edge of the roof should be at or near the ridge crest, and the height of the leading edge above ground should be about the same dimension as the roof length from leading edge to trailing edge.

Keywords: Avalanche control, mountain snow, jet roofs, cornice control.

Dawson, K. L., and T. E. Lang. 1978. Numerical simulation of jet roof geometry for snow cornice control. USDA For. Serv. Res. Pap. RM-206, 19 p. Rocky Mt. For. and Range Exp. Stn., Fort Collins, Colo. 80526.

A numerical solution algorithm is used to study the air flow over a mountain ridge with and without a jet roof located near the ridge crest. For the simple ridge geometry studied the roof should be parallel to the lee slope, the leading edge of the roof should be at or near the ridge crest, and the height of the leading edge above ground should be about the same dimension as the roof length from leading edge to trailing edge.

Keywords: Avalanche control, mountain snow, jet roofs, cornice control.

Dawson, K. L., and T. E. Lang. 1978. Numerical simulation of jet roof geometry for snow cornice control. USDA For. Serv. Res. Pap. RM-206, 19 p. Rocky Mt. For. and Range Exp. Stn., Fort Collins, Colo. 80526.

A numerical solution algorithm is used to study the air flow over a mountain ridge with and without a jet roof located near the ridge crest. For the simple ridge geometry studied the roof should be parallel to the lee slope, the leading edge of the roof should be at or near the ridge crest, and the height of the leading edge above ground should be about the same dimension as the roof length from leading edge to trailing edge.

Keywords: Avalanche control, mountain snow, jet roofs, cornice control.

U.S. DEPT. OF AGRICULTURE
NAT'L AGRIC. LIBRARY
JUN 12 '73